C3 and CD47 dependent mechanisms in the refinement of sensory-motor circuits during spinal cord development

Florez-Paz D[1,2] and Mentis G.Z.[1,2,3]

[1] Center for Motor Neuron Biology and Disease
[2] Dept. of Neurology
[3] Dept. of Pathology and Cell Biology
Columbia University, NY, NY, 10032, USA

Abstract

Overground movement in mammals require the timely and appropriate assembly of spinal sensory-motor circuits. Within spinal cord, sensory neurons, spinal interneurons and motor neurons are key players forming intricate neuronal circuits to ensure proper motor control. The formation of neuronal circuits starts at embryonic period and continues into postnatal development. During this process supernumerary synapses are pruned and refinement of immature circuits occurs, making way for emergence of mature circuits. A major aspect of the sensory-motor circuits' refinement involves the elimination of inappropriate synapses, the molecular mechanisms of which are relatively unknown. We have investigated the molecular mechanisms involved in the elimination of inappropriate proprioceptive synapses from motor neurons by focusing on the classical complement proteins C3 and C1q, as well as the integrin associated protein CD47. Using mouse genetics, viral-mediated neuronal map strategies together with physiological, morphological and molecular biology assays, we found that inappropriate synaptic elimination occurs during early development utilizing both C3 and C1q proteins, but importantly and totally unexpectedly, the CD47 protein. Taken together, our study demonstrates that refinement of immature sensory-motor circuits in the spinal cord is mediated by classical complement dependent mechanisms as well as CD47-dependent mechanisms, uncovering a new role for CD47 as a major player in synapse elimination.

Introduction

Smooth and flawless overground movement in mammals require a timely and carefully orchestrated assembly of spinal sensory-motor circuits. Sensory neurons, spinal interneurons and motor neurons are some of the key players that start forming intricate neuronal circuits during embryonic development (Frank, 1993). These circuits are likely fine-tuned during early postnatal development, at a time where the animal is moving independently (Blankenship and Feller, 2010; Inacio et al., 2016; Robinson et al., 2000). Early formation of neuronal circuits is specified by molecular mechanisms responsible for synaptic formation (Arber, 2012; Jessell, 2000; Lee and Pfaff, 2001). In sensory-motor circuits embedded within the spinal cord, information from the periphery is essential in the generation of smooth movement and key to counteract perturbations in locomotion (Akay et al., 2014; Mayer et al., 2018; Takeoka and Arber, 2019). Proprioceptive fibers are select sensory neurons that convey information about space and time of muscle movement and their activity (de Nooij and Zampieri, 2023; Proske and Gandevia, 2012). Proprioceptive synapses make direct contact with motor neurons (Eccles et al., 1957; Mears and Frank, 1997) as well as with several classes of spinal interneurons (Bikoff et al., 2016; Binder, 1980; Mentis et al., 2010; Siembab et al., 2010).

In mature neuronal circuits, each motor neuron receives proprioceptive synapses originating from the homonymous muscle innervated by the motor neuron, as well as from proprioceptive fibers arising from synergistic muscles (Mears and Frank, 1997; Mendelsohn et al., 2015). While mature motor neurons do not receive proprioceptive inputs from antagonistic muscles, during early development this is not the case. It is debated whether and to what extent, supernumerary sensory synapses are generated during embryonic spinal cord development, leading to formation of inappropriate contacts and irregular neuronal circuits (Chen and Frank, 1999; Frank and Westerfield, 1983; Mentis *et al.*, 2010; Poliak et al., 2016; Seebach and Ziskind-Conhaim, 1994). Although it is currently unclear how and why these inappropriate synapses are formed, they are required to be eliminated for the emergence of mature sensory-motor circuits and proper motor function (Poliak *et al.*, 2016; Seebach and Ziskind-Conhaim, 1994). The molecular mechanisms responsible for the refinement of sensory-motor circuits and synaptic elimination are poorly understood.

A subset of transcription factors (Hoxd9-11) has previously been implicated in irregular formation of select sensory-motor circuits, while other circuits are not affected (Imai et al., 2021). Furthermore, we have recently reported that C1q, the initiating protein of the classical complement cascade, has been implicated in synaptic dysfunction and subsequent elimination in the neurodegenerative disease spinal muscular atrophy (Vukojicic et al., 2019). In addition, C1q has been report to tag synapses in several neuronal circuits, including visual system, cortical circuits and sensory-motor circuits (Fonseca et al., 2017; Stephan et al., 2013; Stevens et al., 2007; Vukojicic *et al.*, 2019).

The opposing scenario responsible for synaptic protection has implicated CD47, an integrin-associated protein, which has been described as a “don’t eat me” signal in the visual

system (Lehrman et al., 2018). Furthermore, under pathological conditions, tumor forming cells overexpress CD47 avoiding engulfment by macrophages (Willingham et al., 2012). In contrast, studies in cortical and hippocampal regions have reported that elimination of SIRPα, the CD47 receptor, contributes to synapse elimination at late but not early stages of development (Ding et al., 2021). Thus, the function of CD47 in synapse elimination is currently unclear.

To elucidate therefore, the molecular mechanisms of synaptic elimination and their potential role in refinement of sensory-motor circuits during early development, we investigated whether activation of the classical complement cascade is causally involved. To do so, we have investigated the involvement of both C1q and C3, its downstream target, in the sensory-motor circuit in the spinal cord during postnatal mouse development. Furthermore, we have studied whether CD47 is acting as a protecting agent or contributes to the process of synaptic removal. To address these questions, we opted to use a well-established proprioceptive-motor neuron circuit responsible for dorsi-flexion and plantar-extension in the hindlimb of neonatal mice. Using virally-mediated neuronal map strategies, mouse genetics to eliminate ubiquitously either C1q, C3 and CD47, or in combination, and together with physiological and morphological assays, we investigated systematically the cascade of events involved in the formation and function of sensory-motor spinal circuits.

In both C3 and C1q knock out mice, we observed a robust increased incidence of proprioceptive synapses within the motor neuron nucleus. We also found a similar observation for the CD47 knock out mice, which is a totally unexpected and surprising result. We determined that this aberrant increase (~30%) of proprioceptive synapses in mutant mice resulted in inappropriate synaptic contacts between flexor proprioceptors and antagonistic (extensor) motor neurons and vice versa. These inappropriate synapses were functional and also were responsible for altered functional characteristics in motor neurons, likely playing an important role in the behavioral phenotype during righting. Taken together, our results shed light into the role of the classical complement cascade in synaptic removal and refinement of sensory-motor circuits in the developing spinal cord. Importantly, CD47 plays a harmful – rather than protective - role in synaptic maintenance and appears to be a major player in synaptic elimination, likely through classical complement-independent mechanisms, involving engulfment of synapses by microglia.

Results

Genetic deletion of C3 or CD47 results in increased numbers of proprioceptive synapses

To investigate the role of C3 and CD47 in the regulation of synaptic contacts in the developing spinal cord, we assessed VGluT1+ proprioceptive synapses in the 4th and 5th lumbar (L4 or L5) spinal segments during early postnatal development in wild type (WT), C3 knock out (C3$^{-/-}$) and CD47 knock out (CD47$^{-/-}$) mice. The somatic and dendritic (0-50μm distance from the soma) coverage of motor neurons (ChAT+) by proprioceptive (VGluT1+) synapses was quantified using immunohistochemistry and confocal microscopy at the postnatal ages, P1, P5 and P10 (Figure 1A; Figure S1A-D). We found that both somatic and dendritic coverage by proprioceptive synapses increased with age in WT motor neurons (Figure 1A-C). At P1, there was no significant difference between WT, C3$^{-/-}$ and CD47$^{-/-}$ mice. In contrast, we observed a significantly higher incidence of proprioceptive synapses in C3$^{-/-}$ mice at P5 and P10 compared with their age-matched counterparts. Additionally, we also found that C1q$^{-/-}$ mice exhibited a higher number of proprioceptive synapses, both at P5 and P10 (Figure S1A-D), in agreement with our previous report that the classical complement cascade is likely involved in synaptic elimination (Vukojicic *et al.*, 2019). Strikingly, CD47$^{-/-}$ mice also revealed a higher incidence of proprioceptive synapses, similar to the that observed in C3$^{-/-}$ mice. This is a totally unexpected finding since CD47 has previously been reported as a "don't eat me" signal, implying that its genetic deletion would have been expected to result in fewer synapses compared to WT mice. Together, these results suggest that synaptic elimination occurs in the spinal cord during postnatal development, employing both classical complement-dependent as well as independent mechanisms.

We next sought to investigate whether the excess number of synapses in both C3$^{-/-}$ and CD47$^{-/-}$ mice are functional. To address this, we performed physiological experiments in which the dorsal-to-ventral root spinal reflexes were quantified using the *ex vivo* spinal cord preparation (Mentis et al., 2011; Vukojicic *et al.*, 2019). We found that the amplitude of the monosynaptically-induced response recorded from the L4 ventral root following stimulation of the homonymous L4 dorsal root was significantly greater in C3$^{-/-}$ and CD47$^{-/-}$ mice compared to WT motor neurons at P10 (Figure 1D,E). The latency of the monosynaptic responses however, did not show any significant difference among the three experimental groups (Figure 1F), demonstrating that the higher number of excess synapses is functional in both C3$^{-/-}$ and CD47$^{-/-}$ mice. Additionally, the amplitude of the monosynaptic responses in C1q$^{-/-}$ mice was also significantly higher compared to age-matched WT controls (Figure S1E-G). To investigate whether the function of the excessive proprioceptive synapses might be prone to synaptic depression, we challenged the synapses at two different frequencies (0.1 and 10Hz). We found no differences in the manner the synaptic response was depressed in C3$^{-/-}$ and CD47$^{-/-}$ mice compared to WT mice, at P5 and P10 (Figure S1K,L). This result suggests that the higher incidence of synapses in both types of mutant mice does not appear to affect the reliability of synaptic neurotransmission. To investigate whether the excessive number of synapses may impact mouse behavior, we quantified the righting time of mice during

the first ten postnatal days. We found that C3$^{-/-}$, but not CD47$^{-/-}$ mice, exhibited significantly longer latencies to right during the first postnatal week compared to WT counterparts (Figure 1G). In addition, C3$^{-/-}$ but not CD47$^{-/-}$ mice, showed differences in body weight compared to WT animals (Figure S1J). Since C3 is a downstream target of C1q in the activation of the classical complement cascade, we next sought to address whether there is any combinatorial influence of both C1q and CD47 deletion in the number of proprioceptive synapses during early development. We found that double knock out mice (C1q$^{-/-}$/CD47$^{-/-}$) did not result in any additional increase of the number of synapses destined to be eliminated (Figure S1H,I). This result suggest that either C1q or CD47 are equally effective in rescuing proprioceptive synapses during early development in the spinal cord.

C3 and CD47 are involved in the elimination of inappropriate synapses

Deletion of C3 or CD47 resulting in a higher incidence of proprioceptive synapses raised the possibility whether the excessive synapses are inappropriate and are destined to be eliminated during early development as part of a refinement process of sensory-motor circuits. To address this, we examined whether proprioceptive fibers originating at the dorsi-flexor muscle Tibialis Anterior (TA) inappropriately contact motor neurons that innervate the biomechanically antagonistic muscle gastrocnemius (Gs; plantar extensor muscle) and vice versa. We first, examined this possibility using a virally-mediated map strategy combined with a combination of genetically modified mice. Similar to a previous report (Balaskas et al., 2019), we used the expression of parvalbumin (Pv) in proprioceptors (Celio, 1990; de Nooij et al., 2013; Ichikawa et al., 1994; Oliver et al., 2021), combined with TdTomato Cre-dependent reporter mice. Animals expressing Pv under FlpO recombination (PV::FlpO) were crossed with a Cre-/FlpO dependent TdTomato reporter (Ai65). The resulting animals (Pv::FlpO$^{+/+}$; Ai65$^{+/+}$) were crossed with C3$^{-/-}$, C1q$^{-/-}$, and C47$^{-/-}$ mouse lines to obtain: *Pv::FlpO*$^{+/+}$*/Ai65*$^{+/+}$*/C3*$^{-/-}$ (denoted as PAC3 for simplicity); *Pv::FlpO*$^{+/+}$*/Ai65*$^{+/+}$*/C1q*$^{-/-}$ (denoted as PAC1q); *Pv::FlpO*$^{+/+}$*/Ai65*$^{+/+}$*/CD47*$^{-/-}$ (denoted as PACD47) strains respectively.

To activate expression of the fluorescent reporter TdTomato in a select group of proprioceptors, we first used a previous reported canine adeno virus expressing Cre (CAV2-CMV-Cre) (Chalif et al., 2022). This virus was injected in the gastrocnemius muscle (Gs) at P0, while an rAAV6/ds-CBH-GFP virus was concomitantly injected in the TA muscle to drive expression of GFP in the somato-dendritic anatomy of TA motor neurons (Figure 2A,B). We investigated putative inappropriate synaptic contacts between Gs proprioceptive fibers and TA motor neurons at P6-7. We found a nearly absent incidence of inappropriate synapses in WT mice, either on the soma or proximal dendrites (Figure 2C-F). In striking contrast, C3$^{-/-}$ and CD47$^{-/-}$ mice exhibited a significantly higher incidence of putative synaptic contacts, verified by colocalization of VGluT1 and Pv+ synapses originating from Gs proprioceptors, on the soma and dendrites of TA motor neurons. To quantify synaptic contacts, we performed intensity profile analysis of all contacts for each confocal image acquired at the single optical plane. Only overlapping VGluT1 and GFP signals above 50% were considered synapses, while 100% overlap between DsRed (motor neuron

postsynaptic site) and VGluT1 signals were considered as inappropriate synapses (Figure 2C-F; Figure S2B). To confirm that labeled (DsRed) proprioceptive synapses innervating homonymous TA motor neurons, we verified that DsRed+ synapses were VGluT1+ and in apposition to ChAT+ motor neurons in L4 sections (Figure S2A).

We found that in mice with C3 and CD47 deletion (PAC3 and PACD47) the incidence of inappropriate synapses was significantly higher, ~55% and ~41% respectively, compared with WT animals (Figure 2D-F). Additionally, we observed that the location of inappropriate synapses was different in each of the two mutant mouse lines. PACD47 mice revealed a significant increase in inappropriate synapses on soma, while PAC3 animals exhibited more inappropriate synapses on proximal dendrites (Figure 2D-F). We also investigated whether there is a preferential direction of inappropriate proprioceptive synapses originating from dorsi-flexor muscles to plantar extensor motor neurons. To address this possibility, we reversed the two viruses injected. Our analysis revealed that inappropriate synapses were also formed between TA proprioceptors to Gs motor neurons in PAC3 mice at the same percentage (Figure S2C,D). Finally, and as expected, PAC1q mice also showed an increase of ~50% of motor neurons with inappropriate synapses (Figure S2E,F). Taken together, these results demonstrate that excessive synapses are formed during early development between proprioceptive neurons and motor neurons innervating muscles of antagonistic biomechanical function. Importantly, we provide morphological evidence that both C3 and CD47 dependent mechanisms are responsible for the elimination of inappropriate synapses during early sensory-motor circuit development in the spinal cord.

Inappropriate synapses are functional and may affect muscle activity

We next investigated whether the inappropriate synapses are functional by performing H-reflex experiments using the *ex vivo* spinal cord-hindlimb preparation (Bikoff *et al.*, 2016; Mentis et al., 2005) at P5 (Figure 3A). In WT mice, stimulation of the common peroneal nerve resulted in a robust M-response and an H-reflex in the TA muscle. As expected, simultaneous recordings from the antagonistic muscle Gs, did not result in any responses (Figure 3B). The nature of neurotransmission responsible for the production of the H-reflex was verified as glutamatergic, since exposure to the NMDA receptor blocker D-AP5 (50μM) and the AMPA/kainate receptor NBQX (20μM) abolished the response (Figure 3B). In $C3^{-/-}$ and $CD47^{-/-}$ mutant mice however, a response with a latency similar to the H-reflex was detected in the antagonistic Gs muscle, following CP nerve stimulation. The amplitude of the H-reflex induced in the homonymous muscle (CP nerve stimulation to TA muscle) did not reveal any significant differences between the three experimental groups (Figure 3C). In contrast, we observed a response in the antagonistic muscle with similar latency to that of the H-reflex in the homonymous muscle (ranged: -1 to +15ms to that of H-reflex; Figure 3C,D) in both $C3^{-/-}$ and $CD47^{-/-}$ mice. This result raised the possibility that inappropriate synapses may be sufficient to activate inappropriately motor neurons that innervate the Gs muscle and likely affect muscle function (Figure 3B, blue arrows in $C3^{-/-}$ and $CD47^{-/-}$ mice).

If classical complement cascade is to be involved in refinement of inappropriate synapses, C1q$^{-/-}$ mice would be expected to also show similar inappropriate responses. C1q$^{-/-}$ mice indeed revealed inappropriate long latency responses similar to those observed in C3$^{-/-}$ mice (Figure S3A-C). These results show that both C3 and CD47 are involved in the pruning of supernumerary synapses, which are likely formed initially through aberrant synapse formation during embryonic and early postnatal development.

To provide unequivocal evidence that inappropriate synapses result in monosynaptic responses and if so, would they have an effect on the excitability of motor neurons, we performed whole cell patch clamp recordings using the *ex vivo* spinal cord hindlimb preparation. The ventral roots L4 and L5 were cut to avoid contamination of the EPSCs by the antidromic action potential that would be induced following CP nerve stimulation. Both L4 and L5 ventral roots were placed in suction electrodes so the patched neuron would be identified as a motor neuron by the presence of an antidromic action potential (Figure S4A,B). TA motor neurons were visually targeted for whole cell intracellular recordings by the presence of CTb-488 injected into the TA muscle at P0 (Figure S4G). EPSPs were induced following proprioceptive fiber stimulation from either TA muscle or the antagonistic Gs muscle (Figure S4A). Appropriate stimulation of each nerve was verified by recording from both TA and Gs muscles (Figure 4A). No differences in CMAPs for any of the muscles latencies were found (Figure S4I).

We found that resting membrane potential of all TA motor neurons was not statistically different across the three experimental groups (Figure S4C). Stimulation of the homonymous nerve (Common Peroneal) resulted in robust monosynaptic EPSCs in all three experimental groups (blue traces in Figure 4B) that had similar amplitude (Figure 4C). In striking contrast, stimulation of the proprioceptive fibers from the antagonistic nerve (tibial nerve) resulted in monosynaptic EPSCs in C3$^{-/-}$ and CD47$^{-/-}$ mutant, but not in WT mice (red traces in Figure 4B). As we have reported previously, the monosynaptic delay in neonatal *ex vivo* spinal cords is ~3.5ms (Mendelsohn *et al.*, 2015). Thus the amplitude of the response after 3.5ms was considered to be of polysynaptic nature. To verify that the responses were of monosynaptic, we performed the jitter test, in which the latency of EPSPs were compared under three different stimulation frequencies (0.1, 0.2 and 1Hz; Figure 4D,E and Figure S5). We found that the coefficient of variation in the latency of the EPSPs were not statistically different under all three different frequencies for the homonymous nerve (Figure 4D) as well as the antagonistic nerve (Figure 4E) confirming all EPSPs were of monosynaptic nature. In support of this, the actual latencies of EPSPs were similar irrespective of the nerve of stimulation (Figure 4F).

To reveal the site of the inappropriate synapses in TA motor neurons from C3$^{-/-}$ and CD47$^{-/-}$ mice, the intracellular solution contained Neurobiotin that we used to reveal *post hoc* the somato-dendritic morphology of the recorded motor neuron (Figure S4G). To do so, we used PAC3 and PACD47 mice that were injected as previously described with a CAV2-CMV-Cre in Gs muscle, but instead of injecting rAAV6/ds-CBH-GFP, we used CTb-488 in TA muscle to increase the number of labelled TA motor neurons. We found that several motor neurons recovered from this type of experiments revealed that several inappropriate synapses were located on the soma of TA

motor neurons (Figure 4H-J). The input resistance of TA motor neurons in C3 and CD47 mice were not statistically different to those TA motor neurons in WT mice (Figure S4D). However, the rheobase current was significantly higher in mutant mice (Figure S4E). The repetitive firing frequency of TA motor neurons appear to be higher in C3 and CD47 mutant mice (Figure S4H) but this difference did not reach statistical significance. Taken together, these results demonstrate that inappropriate synapses in TA motor neurons in $C3^{-/-}$ and $CD47^{-/-}$ mice are functional and have consequences on their firing ability, which may impact muscle activity.

CD47 is expressed in spinal cord neurons but not in glial cells, unlike SIRPα which is expressed in microglia exclusively

To identify the source of CD47 in the spinal cord, we performed RNAscope experiments together with immunohistochemistry assays in P5 and P10 animals. We found that CD47 was produced in motor neurons, identified by ChAT immunoreactivity, but not in microglia identified by Iba1 immunoreactivity, nor astrocytes, identified by GFAP immunoreactivity (Figure 5A,B). In addition, spinal interneurons, located in the intermediate grey matter, identified by NeuN antibodies (Figure 5C) as well proprioceptive neurons in dorsal root ganglia, identified by parvalbumin immunoreactivity, also expressed CD47 (Figure 5D). The CD47 receptor SIRPα was found to be expressed in microglia and proprioceptors, but not in motor neurons (Figure 5E-G).

CD47 tags proprioceptive synapses on motor neurons

We next dwelled into the potential molecular mechanism that may be involved in synaptic pruning and regulated by CD47 activity. CD47 has been described as one of the main molecules involved in synapse protection in certain areas of the brain. However, in complete contrast, the results of our study demonstrate complete the opposite function for CD47. We first investigated whether CD47 expression in the developing spinal cord was involved in synaptic tagging and engulfment of synapses by microglia cells.

We performed immunohistochemistry experiments in which motor neurons were labelled with ChAT antibodies, and visualized proprioceptive synapses with VGluT1 and checked for their association with CD47 immunoreactivity, in L4 and L5 spinal segments at the postnatal ages P0/1, P5 and P10, in WT, $C3^{-/-}$ and $CD47^{-/-}$ mice. Synaptic tagging was evaluated with optical signal intensity profiling, as we previously reported (Vukojicic *et al.*, 2019). CD47 was considered as tagging of VGluT1+ synapses if there is an overlap of their corresponding immunoreactive optical signal (Figure 6D,E). With this criterion in place, we found that CD47 tagged proprioceptive synapses impinging on both the soma and proximal dendrites of motor neurons (Figure 6B,C).The number of tagged VGluT1+ synapses by CD47 was significantly increased at P5 and P10 $C3^{-/-}$ mice, but not at P1 (Figure 6F). A similar observation was observed in $C1q^{-/-}$ mice (Figure S6). We have previously reported that C1q plays a key role in synaptic elimination in the neurodegenerative disease spinal muscular atrophy (or SMA) mediated by microglia, with its RNA

expressed exclusively in microglia (Vukojicic *et al.*, 2019). We therefore, tested the possibility that C1q mRNA puncta may be increased in CD47$^{-/-}$ mice. However, no differences were found at P10 when we quantified C1q mRNA puncta between CD47$^{-/-}$ and WT animals at P5 and P10 (Figure S7A,B). We also found that C3 mRNA puncta was also unchanged between WT and CD47$^{-/-}$ mice (Figure S7C,D). These results indicate that C3 and CD47 mediated synaptic elimination operate via independent mechanisms. These results suggest that the increase in CD47-tagged synapses in C3$^{-/-}$ and C1q$^{-/-}$ knock out mice is likely due to the extra synapses that were not eliminated via classical complement proteins. Thus, CD47 participate in a novel synaptic engulfment mechanism independent of complement proteins.

VGluT1 synaptic residues tagged with CD47 were found within microglia

The classical complement protein C1q, has been demonstrated to be a signaling molecule involved in synaptic pruning in different neuronal circuits. In our study, we have demonstrated that C3 is also implicated in synapse elimination. It has been well established that the C1q-mediated synapse elimination mechanism requires synapse tagging by C1q, which ultimately leads to synaptic engulfment by microglia. To test whether the same synapse needs to be tagged by both C1q and CD47 we performed immunohistochemistry for C1q and CD47 in the spinal cord of newborn (P0) and P5 mice. Remarkably, we found that both CD47 and C1q can tag the same VGluT1 synapse on motor neurons, with an increase of tagging incidence from P0 to P5, coincident with the beginning of the pruning process (Figure 7A,B). Furthermore, we found a robust co-localization of CD47 and C1q puncta associated with a single VGluT1 synapse on motor neurons. Equally important, other synapses were only tagged by either CD47 or C1q (Figure 7A,B). Since synapses tagged by C1q were susceptible to being engulfed by microglia, we investigated the possibility that synapses tagged by C1q and CD47 could also be eliminated. If CD47 played a protective role in synapse elimination, avoiding the engulfment by microglia, it is expected that no CD47 should be found inside microglia. In striking contrast to this hypothesis, we found microglia containing VGluT1 residues tagged by both CD47 and C1q at P0 and P5 but were less frequent at P10 (Figure 7C). Remarkably, we also identify VGluT1 residues associated only with CD47 inside microglia, especially at P5 (Figure 7C). These results suggest that microglia engulf synapses via exclusive CD47 tagging mechanisms as well as a mechanism requiring tagging by both CD47 and C1q. Both these mechanisms could operate independent of each other.

Intriguingly, using immunohistochemistry, we identified association sites of SIRPα and CD47 interacting with parvalbumin+ synapses within the motor neuron nucleus in developing spinal cords (Figure S8A). Additionally, using ChAT antibodies, we confirmed SIRPα and CD47 could also be in contact around the motor neuron membrane (Figure S8B), suggesting putative associations with synapses impinging on motor neurons. This finding strongly suggests that a novel mechanism of synaptic engulfment by microglia is mediated by CD47 and its receptor SIRPα. Together, these results indicate that C1q and its downstream complement protein C3 are not the only proteins associated with VGluT1 synapse engulfment by microglia, but that CD47

could also lead to synapse engulfment. In this sense, SIRPα expression in microglia suggests the role of microglia in CD47 depends on phagocytosis. Most important, CD47 does not protect synapses from engulfment.

Discussion

During early spinal cord development, there is an excessive number of supernumerary proprioceptive synapses that impinge on motor neurons. The result of this higher than normal incidence in synapses is the formation of inappropriate connections between proprioceptive fibers and spinal motor neurons. Proprioceptive neurons of dorsi-flexor muscle origin contact inappropriately motor neurons innervating plantar-extensor muscles and vice versa. Proper assembly of sensory-motor circuits between sensory and motor neurons originating and targeting the same muscle occurs during postnatal development. The synaptic removal and refinement of neuronal circuits for the emergence of mature circuits is achieved through activation of the classical complement pathway, involving C1q and C3. Independently of this process, CD47 is acting independently and in parallel to the classical complement system to remove inappropriate synapses. It acts by activation of microglia through SRIPα signaling. This is a novel and previously unappreciated function of CD47 acting as a key signal in the refinement of sensory-motor circuits.

Complement protein C3 mediates synapse elimination in sensory-motor circuits

We report that in the absence of the classical complement proteins C1q and C3, as well as the integrin associated protein CD47, a ~30% higher incidence of sensory synapses are found within the motor neuron nucleus in the developing lumbar spinal cord. Our results provide robust evidence and demonstrate the transient presence of inappropriate proprioceptive synapses originating from antagonistic muscles as has been postulated by previous studies (Mendelsohn *et al.*, 2015; Seebach and Ziskind-Conhaim, 1994; Vukojicic *et al.*, 2019). It has also been proposed that the elimination of heteronymous synaptic connections occurs in an activity-dependent manner (Mendelsohn *et al.*, 2015). Our study uncovers two independent molecular mechanisms that are causally responsible for the elimination of inappropriate synapses. This elimination process requires activation of the classical complement cascade through C1q and C3 signaling. Additionally, and totally unexpectedly, through CD47, acting independently of the classical complement cascade to contribute in the elimination of supernumerary inappropriate synapses.

The function of C3 in synaptic pruning has also been reported to be involved in the retinogeniculate system (Schafer and Stevens, 2013). Does C3 remove synapses indiscriminately? The answer appears to be negative, since in the hippocampal area, C3 has been implicated to eliminate VGluT2+ synapses, leaving VGluT1+ synapses unaffected (Eric et al., 2020). In our study, we have demonstrated that VGluT1+ synapses are eliminated, suggesting that C3 does not remove selective synapses, raising the possibility the synapse destined to be tagged and ultimately engulfed and removed might be decided by the upstream protein, C1q. An alternate explanation that may help explain the differences in the type of synapses eliminated by C3, may be due to regional differences between brain and spinal cord regions.

An important question regarding the role of inappropriate synapses relates to their function. Do inappropriate synapses function and if so, are they similar to the appropriate ones? Our

functional assays argue that inappropriate synapses function to a similar level as appropriate ones. This observation suggests that C1q or C3 are not merely tagging dysfunctional or silent synapses as part of debris clearance process. Instead, it suggests that inappropriate synapses might express a signal, sensed by the classical complement proteins, that is not present or detectable in the appropriate synapses.

C3 synapse elimination is unlikely to act independently from C1q-directed synaptic elimination

C3 is a downstream target of C1q, since C3 is produced by cleavage of C2 and C4 proteins (Dodds, 2002; Reid, 1985). However, C3 is also produced by the lectin and alternative pathways. However, C3 is unlikely to be activated from either lectin or alternative pathways since these pathways are associated with injection. C3 may activate thought C1q-independent pathways in the context of disease or neuroinflammation, but this is unlikely to occur as part of the normal development. A previous study in the brain demonstrated synapse elimination mediated by C3 activation and interaction with Cx3Cr1 (C3 receptor) from microglia (Cong et al., 2020). In our study, C3 is involved in the elimination of inappropriate synapses similar to the same level observed under C1q knock out conditions. Intriguingly, C3-mediated inappropriate synapse elimination appears to be focused more on somatic synapses rather than dendritic ones, since more inappropriate synapses were found in dendrites of motor neurons in $C3^{-/-}$ mutant mice. This observation may offer an insight into the way the classical complement picks the synapses to be eliminated according to the postsynaptic site.

CD47 does not protect synapses from elimination in spinal sensory-motor circuits

During the last decade, CD47 and its receptor SIRPα have been extensively described as a "don't eat me" signal in the central nervous system, in particular in areas such as hippocampus, retinogeniculate circuit, and cortex (Lehrman *et al.*, 2018; Li et al., 2021; Shui et al., 2022). In striking contrast however, our study demonstrates a novel and totally unexpected function for CD47. Our initial hypothesis was that CD47 would act as a neuroprotective agent and halt synapse elimination as expected from other brain areas. Remarkably, $CD47^{-/-}$ animals exhibited the same levels of synaptic engulfment as the classical complement proteins C3 and C1q. A common assumption about the function of CD47 implicates SIRPα in the protection of synapses from microglia engulfment. To this end, we found in our study that SIRPα is expressed by microglia and contacts CD47 puncta, implying a similar – if not identical - mechanism of CD47 interaction. Our experiments demonstrate that CD47 is a major player in synaptic elimination of inappropriate synapses in the developing spinal cord. The difference of CD47 function in the context of synaptic protection in the retinogeniculate system versus the active role in synaptic pruning in spinal sensory-motor circuits may be due to regional difference. Although CD47 acts similarly to the classical complement proteins in elimination of inappropriate synapses, a distinct difference

between the two mechanisms may be in the postsynaptic site in which synapses are eliminated. For instance, CD47 removed more dendritic synapses as opposed to C3 in which its action mediated removal from mostly somatic synapses. An additional difference could be ascribed to the relative timing of action, whereby we demonstrated that at early stages, microglia engulf VGluT1+ synapses tagged by CD47, with no evidence of engulfment at P10, after the pruning period.

We also observed overexpression of ectopic CD47 in $C1q^{-/-}$ and $C3^{-/-}$ mice at P5. However, there was no increase in synaptic tagging by CD47 in any of the classical complement knock out animals. These observations indicate that the mechanism of CD47 production is not due to over-expression by motor neurons and may be from another source in spinal cord, which does not affect synapse tagging. This lack of difference in motor neuron CD47 expression was confirmed by CD47 mRNA expression in motor neurons. We also described that CD47 was also expressed in interneurons and proprioceptors.

In sum, our study uncovers a surprising novel function for CD47 in synaptic elimination of inappropriate synapses. Additionally, the refinement of immature sensory-motor circuits require either the activation of the classical complement pathway or the action of CD47 to generate mature sensory-motor neuronal circuits.

Methods

Mice

Mice were housed under pathogen-free conditions and all surgical procedures were performed on postnatal mice in accordance with the National Institutes of Health Guidelines on the Care and Use of Animals and approved by the Columbia Animal Care and Use Committee (IACUC). Animals of both sexes were used in this study.

Immunohistochemistry

Dissections of the spinal cords were performed on P7 animals. Mice were anesthetized using 1.2% Avertin (300 mg/kg) by intraperitoneal injection, and transcardial perfusions were performed with PBS followed by paraformaldehyde (PFA) 4%. Post fixation with 4% PFA was performed overnight. The spinal cords were washed out with PBS and immersed in 5% agar, and transverse sections were collected from L4-L5 spinal segments using a vibratome (Leica VT1000S) at 55μm thickness. Sections were incubated in blocking serum containing 10% normal donkey serum in 0.01 M phosphate buffer saline with 0.3% Triton X-100 (PBS-T) for 1 hour. Sections were incubated overnight at room temperature, with primary antibodies at different concentrations in blocking serum. Sections were washed with PBS-T and secondary antibodies were incubated in blocking serum for 3 hours. Finally, sections were washed with PBS and mounted on glass slides using Fluoromount mounting media (Sigma F4680) and subsequently scanned at the confocal microscope.

For quadruple staining, an incubation with donkey anti-goat biotylinated antibody was performed after the incubation with primary antibodies in blocking serum for three hours. After wash with PBS-Triton, Streptavidin – 405 was added as secondary antibody following the protocol for secondary antibodies described above.

The antibody concentrations used in this study are as follows: VGluT1 polyclonal anti-guinea pig (1:2000; custom made) produced by Covance, designed against the epitope (C)GATHSTVQPPRPPPP which lies within the n-terminus of mouse VGluT1. The VGluT1 antibody was validated in VGluT1 knock-out tissue (Fletcher et al., 2017). ChAT polyclonal anti-goat (1:200; Millipore, AB144P). CD47 monoclonal anti-rat (1:500; BD Pharmingen, 555297). GFP polyclonal anti-chicken (1:500; Aves labs, 1020). Ds-red polyclonal anti-rabbit (1:200; Takara, 632496). C1q monoclonal anti-rabbit (1:1000; Abcam, AB182451). Iba1 polyclonal ant-goat (1:500; Abcam, ab5076). Iba1 polyclonal anti-rabbit (1:500. Wako, 019-19741). GFAP polyclonal anti-rabbit (1:500; Dako, Z0334). Donkey anti-goat biotylinated (1:250; Jackson Immuno Research Labs, 705065147). For secondary antibodies from Jackson Immuno Research Labs concentration used was 1:250: DyLight - 405 Streptavidin (016-470-084). DyLight – 488 donkey anti-chicken (703-545-155). Dylight – 488 donkey anti-rabbit (711-545-152). Cy3 donkey

anti-rat (712-165-153). Cy3 donkey anti-rabbit (711-165-152). Cy5 donkey anti-guinea pig (7066-175-148). Cy5 donkey anti-rabbit (711-175-152). Cy5 donkey anti-chicken (703-175-155).

Labelling of muscle selective motor neurons and proprioceptors

In order to label specifically motor neurons innervating the tibialis anterior (TA) or gastrocnemius (Gs) muscles and the proprioceptor to motor neuron synapses from antagonistic muscles, we used a modified protocol reported by Balaskas and colleagues (Balaskas *et al.*, 2019). Briefly, two mouse strains were crossed, parvalbumin (Pv)-directed FlpO recombinase (Pv::FlpO), Jackson Laboratory (B6.Cg-*Pvalb*$^{tm4.1(flpo)Hze}$/J) (ref. 022730), and Cre and Flp-dependent TdTomato reported mouse [Ai65 (RCFL-tdt)-D], Jackson Laboratory (B6;129S-*Gt(ROSA)26Sor*$^{tm65.1(CAG\text{-}tdTomato)Hze}$/J) (ref. 021875) to obtain Pv::FlpO;Ai65 mice. These animals were crossed with C3$^{-/-}$, C1q$^{-/-}$, and CD47$^{-/-}$ animals to obtain Pv::FlpO;Ai65;C1q$^{-/-}$, Pv::FlpO;Ai65;C3$^{-/-}$, and Pv::FlpO;Ai65;CD47$^{-/-}$ strains respectively. Only homozygous animals for all the genes were used for experiments, and Pv::FlpO;Ai65 was used as control. Labeling of motor neurons innervating TA muscle and proprioceptors innervating Gs was performed as follows: newborn (P0-P1) pups were anesthetized with isoflurane 5% and 1liter/min of O2. 3 mm incisions were performed unilaterally in the right hindlimb at the front and back side of the hindlimb to expose the TA and Gs respectively. ~1 µl of the virus was injected using a fine glass micropipette. The viruses injected were: in TA rAAV6/ds-CBH-GFP (Vector core of the University of North Carolina, USA) to label TA motor neurons. CAV2-CMV-Cre virus in Gs (Plateforme de Vectorologie de Montpellier, France) to flip the expression of Ai65 gene only in parvalbumin-positive Gs innervating cells; this allowed us to specifically label proprioceptors originating in a select muscle.

Quantification of synapse number and CD47 tagging

Images from immunohistochemistry experiments were obtained using SP8 Leica confocal microscope (Leica Microsystems). Z-stacks images of 20-30 µm at 3.5 µm interval, were obtained using a 40x oil immersion objective, at 4096 x 4096 dpi resolution. Images were analyzed using ImageJ software (National Institute of Health). Quantification was performed using only neurons whose somata were completely covered by the Z-stack and only synapses on the soma were quantified. For synapses on dendrites, the first 50 µm dendritic compartment from the soma was included in the analysis. Synapses were labeled as “tagged” by CD47 only or CD47 and C1q when their protein expression colocalized with the synaptic signal, identified by VGlut1, and confirmed by an overlap using intensity profiling. Analysis of the total number of synapses on somata and dendrites and the number of synapses tagged were used to obtain the percentage of tagged synapses.

RNAscope assay

Spinal cords were obtained at P1, P5, and P10 pups as was described for immunohistochemistry experiments. After overnight 4% post-fixation, the tissue was immersed in 10% sucrose in PBS at 4˚C for 72 h. The tissue containing L4-L6 lumbar enlargement was obtained and frozen in Optimal Cutting Temperature media (OCT) and sections of 14 – 20 µm were cut in a cryostat (Leica SM3050S) and mounted on SuperFrost Plus slides (Fisher Scientific). RNAscope® Multiplex Fluorescent Detection Kit v2 (ACD BioTchne; Cat 323110) was used for detection. Slides were incubated at 60˚C for 30 min and post-fixed with 4% PFA. Slides were dehydrated using ethanol dilutions of 50%, 70%, and 100% for 5 min each, followed by incubation with hydrogen peroxide (ACD BioTechne. Ref. 322335) for 10 min, after washing out with distilled H_2O sections were embedded in 100% alcohol for 3 min. Protease Plus (ACD BioTechne. Ref. 322331) was added and slides were incubated at 40˚C for 30 min. Hybridization was performed by adding a specific probe for each gene and incubating the slides for 2h at 40˚C. Slides were washed with 1X wash buffer (ACD BioTechne. Ref. 310091) and incubated at room temperature overnight in 1X saline sodium citrate (SSC). The following day, slides were incubated with Hybridize AMP1, Hybridize AMP2, and Hybridize AMP3 for 30 min at 40˚C each. Finally, HRP signals were developed using HRP-C1, HRP-C2, or HRP-C3 depending on the channel of each probe, and incubated for 15 min at 40˚C. TSA fluorescein, TSA Cy3 or TSA Cy5 (PerkinELmer. Ref. NEL760001KT) were used to reveal the probe following company indications. To stop the hybridization, slides were incubated for 15 min at 40˚C with an HRP blocker (ACD BioTechne. Ref. 323107), and mounted using Fluoromount mounting media (Sigma F4680).

For double RNAscope – immunohistochemistry assays, immunohistochemistry protocol was performed as indicated above starting with the blocking using blocking serum after the incubation with HRP blocker. Images were taken between 1 and 15 days after the experiment.
Probes used were obtained from ACD BioTchne and the protocol for dilution was followed as indicated by the company. Probes were, C1q (ACD BioTechne. Ref. 441221-C3), CD47 (ACD BioTechne. Ref. 515461-C2), and SIRPα (ACD BioTechne. Ref. 527228-C1).

Genotype

DNA extraction was done using tail tissue incubated at 55˚C for 60 min in 0.05% Proteinase K (Thermo Fisher Scientific. Ref. EO0491), diluted in tail lysis buffer containing: Tris 1M, EDTA 0.5M, NaCL 0.2M, SDS 0.07M. Samples were diluted at 1:20 in H_2O. Genotype protocols for PV::FlpO, Ai65 (RCFL-tdt), $C3^{-/-}$, $C1q^{-/-}$, and $CD47^{-/-}$ animals were followed as described in Jackson laboratory website (www.jax.org). For all animals universal PCR reaction was used as follows: 12.5 µl of GoTaq Hot Start Green Master Mix (Promega), 0.5 µl of each primer (25 µM; Sigma), and 4 µl of 1:20 diluted lysed tail DNA in a final volume of 25 µl using dH2O. For Pv::FlpO, and Ai65 (RCFL-tdt)-D and $CD47^{-/-}$ alleles products were amplified using the following thermal cycling method: 94°C for 2 min, followed by 10 cycles of 94°C for 20 sec,

65°C for 15 sec, 68°C for 10 sec, then 28 cycles of 94°C for 15 sec, 60°C for 15 sec, 72°C for 10 sec, and followed by 72°C for 2 min. For $C3^{-/-}$ alleles products were amplified using the following thermal cycling method: 94°C for 3 min, followed by 12 cycles of 94°C for 20 sec, 64°C for 30 sec, 72°C for 35 sec, then 25 cycles of 94°C for 20 sec, 58°C for 30 sec, 72°C for 35 sec, and followed by 72°C for 2 min. For $C1q^{-/-}$ alleles products were amplified using the following thermal cycling method: 94°C for 4 min, followed by 35 cycles of 94°C for 1 min, 57°C for 30 sec, 72°C for 30 sec, and followed by 72°C for 10 min.

Customized primers used are listed as follows: for C1q, mutant 5'-3' GGGGATCGGCAATAAAAAGAC, WT 5'-3' GGGGCCTGTGATCCAGACAG, 3'-5' common ACCAATCGCTTCTCAGGACC; with a product of WT ~330 and mutant ~120. For C3, mutant 3'-5' TGGGCTCTATGGCTTCTGAG, WT 3'-5' CACCTTACAGCACTCCCACA, 5'-3' common GAAGTGGAAGTTGAACAAATCG; with a product of WT ~300 and mutant ~199. For Ai65 (RCFL-tdt)-D, in separate reactions, WT 5'-3' ACGGGCAGTAGGGCTGAG, 3'-5' AGCCTGCCCAGAAGACTCC, and mutant 5'-3' GCAATAGCATCACAAATTTCA C, 3'-5' TCTAGCTTGGGCTGCAGGT. For PV::FlpO, WT 5'-3' GGATGCTTGCCGAAGATAAG, mutant 5'-3' CTGAGCAGCTACATCAAC AGG, common 3'-5' TGTTTCTCCAGCATTTCCAG. For CD47, WT 3'-5' CACCTTACAGCACTCCCACA, mutant 3'-5' TGGGCTCTATGGCTTCTGAG, and common 5'-3' GAAGTGGAAGTTGAACAAATCG.

Electrophysiology

The *ex vivo* spinal cord preparation used in this study has been described in previous publications (Fletcher et al., 2017; Mentis et al., 2011). Briefly, neonatal pups were decapitated and the spinal cord wa extracted in artificial cerebrospinal fluid (aCSF) at ~12˚C, and oxygenated with 95%O_2/5%CO_2. aCSF contains in mM: 128.35 NaCl, 4 KCl, 0.58 $NaH_2PO_4.H_20$, 21 $NaHCO_3$, 30 D-Glucose, 1.5 $CaCl_2.H_20$, and 1 $MgSO_4.7H_20$. The spinal cord was transferred to the recording chamber with aCSF perfusion (~10 ml/min) at room temperature (~22˚C). Suction electrodes were placed in the dorsal root or ventral root for either stimulation or recording.

The stimulus threshold was defined as the minimal current necessary to evoke a response in the ventral root in three out of five trials, with 0.2 ms of stimulation duration. The stimulus was delivered by a constant current stimulus isolator (A365 - WPI, Sarasota, FL). The recordings were amplified 1000x (Cyberamp, Molecular Devices), fed to an A/D interface (Digidata 1320A, Molecular Devices), and acquired at 50kHZ using Clampex (v10, Molecular Devices). Data were then analyzed offline using Clampfit (Molecular Devices). Only monosynaptic responses over 1mV amplitude were considered for analysis. A series of 10 stimuli were performed at 0.1, 0.2, 1 and 10 Hz. Monosynaptic amplitude was measured as the average of 10 single responses at 0.1 Hz.

Statistical analysis

Statistical analysis was performed using Graphpad software (PRISM version 6.01.). Comparisons were performed by either Student's t-test or One-Way ANOVA when conditions of normality and homoscedasticity were respected. If violated, Mann–Whitney-Wilcoxon and Kruskal-Wallis tests were used as non-parametric tests. Post-hoc multiple comparison methods are indicated in the Results and figure legends when necessary. A statistical significance was considered $P<0.05$. Results are expressed as means ± standard error of the mean (SEM).

References

1. Akay, T., Tourtellotte, W.G., Arber, S., and Jessell, T.M. (2014). Degradation of mouse locomotor pattern in the absence of proprioceptive sensory feedback. Proc Natl Acad Sci U S A *111*, 16877-16882. 10.1073/pnas.1419045111.

2. Arber, S. (2012). Motor circuits in action: specification, connectivity, and function. Neuron *74*, 975-989. 10.1016/j.neuron.2012.05.011.

3. Balaskas, N., Abbott, L.F., Jessell, T.M., and Ng, D. (2019). Positional Strategies for Connection Specificity and Synaptic Organization in Spinal Sensory-Motor Circuits. Neuron *102*, 1143-1156 e1144. 10.1016/j.neuron.2019.04.008.

4. Bikoff, J.B., Gabitto, M.I., Rivard, A.F., Drobac, E., Machado, T.A., Miri, A., Brenner-Morton, S., Famojure, E., Diaz, C., Alvarez, F.J., et al. (2016). Spinal Inhibitory Interneuron Diversity Delineates Variant Motor Microcircuits. Cell *165*, 207-219. 10.1016/j.cell.2016.01.027.

5. Binder, M.D. (1980). Topographic organization of monosynaptic reflexes in the cat spinal cord. Neurosci Lett *20*, 121-124. 10.1016/0304-3940(80)90132-9.

6. Blankenship, A.G., and Feller, M.B. (2010). Mechanisms underlying spontaneous patterned activity in developing neural circuits. Nat Rev Neurosci *11*, 18-29. 10.1038/nrn2759.

7. Celio, M.R. (1990). Calbindin D-28k and parvalbumin in the rat nervous system. Neuroscience *35*, 375-475. 10.1016/0306-4522(90)90091-h.

8. Chalif, J.I., Martinez-Silva, M.L., Pagiazitis, J.G., Murray, A.J., and Mentis, G.Z. (2022). Control of mammalian locomotion by ventral spinocerebellar tract neurons. Cell *185*, 328-344 e326. 10.1016/j.cell.2021.12.014.

9. Chen, H.H., and Frank, E. (1999). Development and specification of muscle sensory neurons. Curr Opin Neurobiol *9*, 405-409. 10.1016/S0959-4388(99)80061-0.

10. Cong, Q., Soteros, B.M., Wollet, M., Kim, J.H., and Sia, G.M. (2020). The endogenous neuronal complement inhibitor SRPX2 protects against complement-mediated synapse elimination during development. Nat Neurosci *23*, 1067-1078. 10.1038/s41593-020-0672-0.

11. de Nooij, J.C., Doobar, S., and Jessell, T.M. (2013). Etv1 inactivation reveals proprioceptor subclasses that reflect the level of NT3 expression in muscle targets. Neuron *77*, 1055-1068. 10.1016/j.neuron.2013.01.015.

12. de Nooij, J.C., and Zampieri, N. (2023). The making of a proprioceptor: a tale of two identities. Trends Neurosci. 10.1016/j.tins.2023.09.008.

13. Ding, X., Wang, J., Huang, M., Chen, Z., Liu, J., Zhang, Q., Zhang, C., Xiang, Y., Zen, K., and Li, L. (2021). Loss of microglial SIRPalpha promotes synaptic pruning in preclinical models of neurodegeneration. Nat Commun *12*, 2030. 10.1038/s41467-021-22301-1.

14. Dodds, A.W. (2002). Which came first, the lectin/classical pathway or the alternative pathway of complement? Immunobiology *205*, 340-354. 10.1078/0171-2985-00137.

15. Eccles, J.C., Eccles, R.M., and Lundberg, A. (1957). The convergence of monosynaptic excitatory afferents on to many different species of alpha motoneurones. J Physiol *137*, 22-50.

16. Eric, W.S., Gang, L., Sun-Lim, C., Liam, T.R., Lijia, Z., Fuzi, J., Ashish, K., Junhui, W., John, G., and Graham, L.C. (2020). Complement C3-dependent glutamatergic synapse elimination in the developing hippocampus is region- and synapse-specific. bioRxiv, 2020.2005.2020.106930. 10.1101/2020.05.20.106930.

17. Fletcher, E.V., Simon, C.M., Pagiazitis, J.G., Chalif, J.I., Vukojicic, A., Drobac, E., Wang, X., and Mentis, G.Z. (2017). Reduced sensory synaptic excitation impairs motor neuron function via Kv2.1 in spinal muscular atrophy. Nat Neurosci *20*, 905-916. 10.1038/nn.4561.

18. Fonseca, M.I., Chu, S.H., Hernandez, M.X., Fang, M.J., Modarresi, L., Selvan, P., MacGregor, G.R., and Tenner, A.J. (2017). Cell-specific deletion of C1qa identifies microglia as the dominant source of C1q in mouse brain. J Neuroinflammation *14*, 48. 10.1186/s12974-017-0814-9.

19. Frank, E. (1993). New life in an old structure: the development of synaptic pathways in the spinal cord. Curr Opin Neurobiol *3*, 82-86. 10.1016/0959-4388(93)90039-2.

20. Frank, E., and Westerfield, M. (1983). Development of sensory-motor synapses in the spinal cord of the frog. J Physiol *343*, 593-610. 10.1113/jphysiol.1983.sp014912.

21. Ichikawa, H., Deguchi, T., Nakago, T., Jacobowitz, D.M., and Sugimoto, T. (1994). Parvalbumin, calretinin and carbonic anhydrase in the trigeminal and spinal primary neurons of the rat. Brain Res *655*, 241-245. 10.1016/0006-8993(94)91620-9.

22. Imai, F., Adam, M., Potter, S.S., and Yoshida, Y. (2021). HoxD transcription factors define monosynaptic sensory-motor specificity in the developing spinal cord. Development *148*. 10.1242/dev.191122.

23. Inacio, A.R., Nasretdinov, A., Lebedeva, J., and Khazipov, R. (2016). Sensory feedback synchronizes motor and sensory neuronal networks in the neonatal rat spinal cord. Nat Commun *7*, 13060. 10.1038/ncomms13060.

24. Jessell, T.M. (2000). Neuronal specification in the spinal cord: inductive signals and transcriptional codes. Nat Rev Genet *1*, 20-29. 10.1038/35049541.

25. Lee, S.K., and Pfaff, S.L. (2001). Transcriptional networks regulating neuronal identity in the developing spinal cord. Nat Neurosci *4 Suppl*, 1183-1191. 10.1038/nn750.

26. Lehrman, E.K., Wilton, D.K., Litvina, E.Y., Welsh, C.A., Chang, S.T., Frouin, A., Walker, A.J., Heller, M.D., Umemori, H., Chen, C., and Stevens, B. (2018). CD47 Protects Synapses from Excess Microglia-Mediated Pruning during Development. Neuron *100*, 120-134 e126. 10.1016/j.neuron.2018.09.017.

27. Li, J., Brickler, T., Banuelos, A., Marjon, K., Shcherbina, A., Banerjee, S., Bian, J., Narayanan, C., Weissman, I.L., and Chetty, S. (2021). Overexpression of CD47 is associated with brain overgrowth and 16p11.2 deletion syndrome. Proc Natl Acad Sci U S A *118*. 10.1073/pnas.2005483118.

28. Mayer, W.P., Murray, A.J., Brenner-Morton, S., Jessell, T.M., Tourtellotte, W.G., and Akay, T. (2018). Role of muscle spindle feedback in regulating muscle activity strength during walking at different speed in mice. J Neurophysiol *120*, 2484-2497. 10.1152/jn.00250.2018.

29. Mears, S.C., and Frank, E. (1997). Formation of specific monosynaptic connections between muscle spindle afferents and motoneurons in the mouse. J Neurosci *17*, 3128-3135.

30. Mendelsohn, A.I., Simon, C.M., Abbott, L.F., Mentis, G.Z., and Jessell, T.M. (2015). Activity Regulates the Incidence of Heteronymous Sensory-Motor Connections. Neuron *87*, 111-123. 10.1016/j.neuron.2015.05.045.

31. Mentis, G.Z., Alvarez, F.J., Bonnot, A., Richards, D.S., Gonzalez-Forero, D., Zerda, R., and O'Donovan, M.J. (2005). Noncholinergic excitatory actions of motoneurons in the neonatal mammalian spinal cord. Proc Natl Acad Sci U S A *102*, 7344-7349. 10.1073/pnas.0502788102.

32. Mentis, G.Z., Alvarez, F.J., Shneider, N.A., Siembab, V.C., and O'Donovan, M.J. (2010). Mechanisms regulating the specificity and strength of muscle afferent inputs in the spinal cord. Ann N Y Acad Sci *1198*, 220-230. 10.1111/j.1749-6632.2010.05538.x.

33. Mentis, G.Z., Blivis, D., Liu, W., Drobac, E., Crowder, M.E., Kong, L., Alvarez, F.J., Sumner, C.J., and O'Donovan, M.J. (2011). Early functional impairment of sensory-motor connectivity in a mouse model of spinal muscular atrophy. Neuron *69*, 453-467. 10.1016/j.neuron.2010.12.032.

34. Oliver, K.M., Florez-Paz, D.M., Badea, T.C., Mentis, G.Z., Menon, V., and de Nooij, J.C. (2021). Molecular correlates of muscle spindle and Golgi tendon organ afferents. Nat Commun *12*, 1451. 10.1038/s41467-021-21880-3.

35. Poliak, S., Norovich, A.L., Yamagata, M., Sanes, J.R., and Jessell, T.M. (2016). Muscle-type Identity of Proprioceptors Specified by Spatially Restricted Signals from Limb Mesenchyme. Cell *164*, 512-525. 10.1016/j.cell.2015.12.049.

36. Proske, U., and Gandevia, S.C. (2012). The proprioceptive senses: their roles in signaling body shape, body position and movement, and muscle force. Physiol Rev *92*, 1651-1697. 10.1152/physrev.00048.2011.

37. Reid, K.B. (1985). Application of molecular cloning to studies on the complement system. Immunology *55*, 185-196.

38. Robinson, S.R., Blumberg, M.S., Lane, M.S., and Kreber, L.A. (2000). Spontaneous motor activity in fetal and infant rats is organized into discrete multilimb bouts. Behav Neurosci *114*, 328-336. 10.1037//0735-7044.114.2.328.

39. Schafer, D.P., and Stevens, B. (2013). Phagocytic glial cells: sculpting synaptic circuits in the developing nervous system. Curr Opin Neurobiol *23*, 1034-1040. 10.1016/j.conb.2013.09.012.

40. Seebach, B.S., and Ziskind-Conhaim, L. (1994). Formation of transient inappropriate sensorimotor synapses in developing rat spinal cords. J Neurosci *14*, 4520-4528.

41. Shui, M., Sun, Y., Lin, D., Xue, Z., Liu, J., Wu, A., and Wei, C. (2022). Anomalous Levels of CD47/Signal Regulatory Protein Alpha in the Hippocampus Lead to Excess Microglial Engulfment in Mouse Model of Perioperative Neurocognitive Disorders. Front Neurosci *16*, 788675. 10.3389/fnins.2022.788675.

42. Siembab, V.C., Smith, C.A., Zagoraiou, L., Berrocal, M.C., Mentis, G.Z., and Alvarez, F.J. (2010). Target selection of proprioceptive and motor axon synapses on neonatal V1-derived Ia inhibitory interneurons and Renshaw cells. J Comp Neurol *518*, 4675-4701. 10.1002/cne.22441.

43. Stephan, A.H., Madison, D.V., Mateos, J.M., Fraser, D.A., Lovelett, E.A., Coutellier, L., Kim, L., Tsai, H.H., Huang, E.J., Rowitch, D.H., et al. (2013). A dramatic increase of C1q protein in the CNS during normal aging. J Neurosci *33*, 13460-13474. 10.1523/jneurosci.1333-13.2013.

44. Stevens, B., Allen, N.J., Vazquez, L.E., Howell, G.R., Christopherson, K.S., Nouri, N., Micheva, K.D., Mehalow, A.K., Huberman, A.D., Stafford, B., et al. (2007). The classical complement cascade mediates CNS synapse elimination. Cell *131*, 1164-1178. 10.1016/j.cell.2007.10.036.

45. Takeoka, A., and Arber, S. (2019). Functional Local Proprioceptive Feedback Circuits Initiate and Maintain Locomotor Recovery after Spinal Cord Injury. Cell Rep *27*, 71-85 e73. 10.1016/j.celrep.2019.03.010.

46. Vukojicic, A., Delestree, N., Fletcher, E.V., Pagiazitis, J.G., Sankaranarayanan, S., Yednock, T.A., Barres, B.A., and Mentis, G.Z. (2019). The Classical Complement Pathway Mediates Microglia-Dependent Remodeling of Spinal Motor Circuits during Development and in SMA. Cell Rep *29*, 3087-3100 e3087. 10.1016/j.celrep.2019.11.013.

47. Willingham, S.B., Volkmer, J.P., Gentles, A.J., Sahoo, D., Dalerba, P., Mitra, S.S., Wang, J., Contreras-Trujillo, H., Martin, R., Cohen, J.D., et al. (2012). The CD47-signal regulatory protein alpha (SIRPa) interaction is a therapeutic target for human solid tumors. Proc Natl Acad Sci U S A *109*, 6662-6667. 10.1073/pnas.1121623109.

Figure legends

<u>Figure 1</u>. Genetic deletion of C3 or CD47 exhibit a higher incidence of VGlut1+ synapses on spinal motor neurons. A) Confocal images from L4 motor neurons at P5. Motor neurons (blue) and VGluT1 synapses (white) in WT, $C3^{-/-}$ and $CD47^{-/-}$ mice. c**.** Insets show higher magnification a motor neuron and VGluT1 synapses. **B)** Number of VGluT1 synapses per motor neuron soma at P1, P5 and P10 (N=3 mice per group). Number of somata: WT, P1, n=18; P5, n=14; P10, n=16; $C3^{-/-}$, P1, n=18; P5, n=17; P10 n=16; $CD47^{-/-}$, P1, n=15; P5, n=10; P10, n=12. **C)** Synaptic density in 0-50 μm proximal dendrites (N=3 mice per group). Number of dendrites: WT, P1, n=30; P5, n=24; P10, n=30; $C3^{-/-}$, P1, n=30; P5, n=30; P10, n=30; $CD47^{-/-}$, P1, n=30; P5, n=20; P10, n=30. *$p < 0.05$, **$p < 0.001$, ***$p < 0.001$; one-way ANOVA multiple comparisons with Bonferroni's test. **D)** Ventral root (L4) responses following dorsal root (L4) stimulation. Red trace is the average of the first five trials (in grey). Arrowheads indicate stimulus artifacts. Blue arrows indicate peak amplitude in the averaged response. **E)** Amplitude of spinal reflexes at P5. WT, N=6; $C3^{-/-}$, N=4; $CD47^{-/-}$, N=4. *$p < 0.05$, one-way ANOVA multiple comparisons with Bonferroni's test. **F)** Latency of responses for the same group as in (**E**). **G)** Righting times across the first ten postnatal days for WT, $C3^{-/-}$ and $CD47^{-/-}$ mice.

<u>Figure 2</u>. Inappropriate synapses on motor neurons formed by proprioceptive fibers originating in antagonistic muscles in $C3^{-/-}$ and $CD47^{-/-}$ mice. A) Fluorescent and transmitted light photograph of the hindlimb injected (at P0) with CAV2-CMV-Cre virus in gastrocnemius and rAAV6/ds-CBH-GFP virus in TA, at P5. **B)** Confocal image of an inappropriate synapse. Inset shows the line profile used as a criterion. The signal intensity is shown in the graph for each of the three immunoreactive signals. Gs proprioceptive fibers labeled with DsRed (red), TA motor neuron dendrites (green) and VGlut1 synapses (blue). **C)** Confocal images of L4 TA MN from PV::FlpO;Ai65 (WT; top), PV::FlpO;Ai65;$C3^{-/-}$ ($PAC3^{-/-}$; middle), and PV::FlpO;Ai65;$CD47^{-/-}$ ($PACD47^{-/-}$; bottom) mice. Z-stack 3.5 μm, amplified image of dendrite from yellow dotted line (left), and examples from somas (center). Yellow arrows highlight inappropriate synapses. Scale bar 20 μm. Inserts from dendrite inappropriate synapses examples (right). Scale bar 2 μm. **D)** Percentage of inappropriate synapses formation including somata and dendrites; WT, N=3; $C3^{-/-}$, N=3; $CD47^{-/-}$, N=2 from P5-P7 mice. **E)** Normalized number of inappropriate somatic synapses per number of cells labeled. **F)** As in (E) for dendritic inappropriate synapses (WT, n=5; $C3^{-/-}$, n=6; $CD47^{-/-}$, n=4). *$p < 0.05$, **$p < 0.001$, ***$p < 0.001$; one-way ANOVA multiple comparisons with Dunnett's test.

<u>Figure 3</u>. Inappropriate synapses induce H reflex responses in antagonistic muscles. A) Schematic illustration for extracellular recordings using the *ex vivo* hindlimb preparation. Electrodes used to record TA and Gs EMG activity, and suction electrodes to stimulate Common Peroneal (CP) and Tibial (T) nerves. **B)** EMG recordings from homonymous muscles (TA, top traces) and antagonistic muscles (Gs, bottom traces) following CP nerve stimulation. Left, is from

a WT spinal cord in aCSF (control) solution. Second from left, after exposure to NBQX (20 μM) and D-AP5 (50 μM). Right traces from $C3^{-/-}$ and $CD47^{-/-}$ mice in control aCSF. Red traces show the average of the first five trials (grey). Arrowhead shows stimulation artifact. Green arrows point to homonymous H-reflex, while blue arrows point to inappropriate H-reflexes. **C)** Amplitude of EMG response for homonymous H-reflex (left) and antagonistic H-reflex (right). Each data point corresponds to a recording from Gs or TA muscle; WT, N=6; $C3^{-/-}$, N=10; $CD47^{-/-}$, N=6. *$p < 0.05$, **$p < 0.001$; one-way ANOVA multiple comparisons with Bonferroni's test. **D)** Latency of M-responses, homonymous H-reflex and antagonistic H-reflex.

<u>Figure 4</u>. Intracellular EPSCs demonstrate functionality of inappropriate synapses. A) Spinal cord-hindlimb *ex vivo* preparation experiments for whole cell patch-clamp from TA motor neurons, plus extracellular Compound Muscle Action Potential (CMAP) recordings from Gs and TA muscles. Traces represent homonymous (TA) (top traces) and antagonistic (GA) (bottom traces) muscle responses after CP and T nerve stimulations, respectively. Traces correspond to the first five responses at 0.1 Hz. **B)** Whole-cell responses from TA motor neurons correspond to the same experiments shown above. EPSC responses correspond to the mean of first five responses. EPSC following homonymous CP nerve stimulus (blue), and after antagonistic Tibial nerve stimulation (red). Dot lines depict 3.5 ms as the time for monosynaptic activation. Right traces represent I-V relationships from the same motor neuron. **C)** Amplitude of EPSC following CP and Tibial nerve stimulation for WT, $C3^{-/-}$ and $CD47^{-/-}$ mice. WT, N=7; $C3^{-/-}$, N=5; $CD47^{-/-}$, N=7. **D)** Coefficient of variation of latency of responses induced at different frequencies following CP nerve stimulation. WT, N=7; $C3^{-/-}$, N=5; $CD47^{-/-}$, N=7. **E)** Similar to (D) but following tibial nerve stimulation. **F)** H-reflex latencies in WT (blue), $C3^{-/-}$ (green) and $CD47^{-/-}$ (purple) mice following CP and tibial nerve stimulation. **G)** Fluorescence and transmitted light photograph of the spinal cord-hindlimb *ex vivo* spinal cord preparation. Gs in red; TA in green. CP nerve is shown by red arrow, while Tibial nerve is shown by the yellow arrow. Sciatic nerve is shown by white arrow. **H-J)** Example of a PV::FlpO;Ai65;$C3^{-/-}$ **(I)**, and PV::FlpO;Ai65;$CD47^{-/-}$ **(J)**, injected with CAV2-CMV-Cre virus in GA and CTB488 in TA. Confocal images of the TA recorded motor neuron for each mouse line from experiments in A and B. Quadruple immunostaining against VGluT1 (red), DsRed (green), Neurobiotin (blue), and injected CTB488 (magenta). Merged image 3.5 μm from Z-stack (top), and higher mag image showing soma of motor neuron with inappropriate synapse (white arrows).

<u>Figure 5</u>. CD47-mRNA is expressed in spinal cord neurons, while microglia express SRIPα. A) RNAscope experiments combined with immunohistochemistry assays. Z-stack confocal projections (total distance 3.5 μm) from a P5 L4 spinal cord; ChAT (blue), Iba1 (red) and CD47 (green), from WT, $CD47^{-/-}$. Scale bar 10 μm (right) and Scale bar 5 μm (middle and left). **B)** Single optical plane of a ChAT+ motor neuron (blue), GFAP (red) and CD47 (green). Scale bar 10 μm (right) and Scale bar 5 μm (middle and left). **C)** Confocal image from NeuN (blue) and ChAT (red) immunoreactivity combined with CD47-mRNA (green). Scale bar 50 μm. **D)** DRGs confocal

image of Parvalbumin (blue), DAPI (white) and CD47 mRNA (green). Scale bar 50 μm. **E)** Confocal image of Parvalbumin (blue), DAPI (white) and SIRPa mRNA (red). Scale bar 50 μm. **F)** Spinal cord Confocal image showing ChAT (blue), Iba1 (green) and SIRPα mRNA (red) signals. Scale bar 50 μm. **G)** Single optical plane confocal image, showing Iba1 (blue), SIRPα (green) and CD47 (red). Scale bar 5 μm.

Figure 6. CD47 tags VGluT1 synapses in spinal sensory-motor circuits. A) Confocal image showing VGluT1 (red), CD47 (green) and ChAT (blue) immunoreactivity from WT, $C3^{-/-}$ and $CD47^{-/-}$ mice. Scale bar 50 μm. **B)** VGluT1+ synapse (red) is tagged by CD47 (green) apposed on the soma to a motor neuron (ChAT, blue). A line intensity profile is shown with a dotted line. Scale bar 50 μm. **C)** Similar to (B) but for a dendritic synapse. Scale bar 5 μm. **D,E)** Line intensity profiles as shown by dotted lines in (B) and (C) respectively. **F)** Percentage of somatic synapses tagged by CD47. **G)** Percentage of dendritic synapses tagged by CD47.

Figure 7. Microglia engulf synapses tagged by C1q, CD47 or together. A) Orthogonal view of images of immunohistochemistry experiments for C1q (green), CD47 (red) VGlut1 (grey) and ChAT (blue). Circles indicate VGlut1 synapses tagged by CD47 (red), C1q (green) or CD47+C1q (yellow). Inserts represent higher magnifications of the orthogonal views, yellow arrows indicate double tagging of VGluT1 synapsis with CD47 and C1q. Scale bar 10 μm. **B)** Quantification of VGluT1 synapses double-tagged at P0 and P5. $**p < 0.001$; Unpaired t-test. **C)** Representative confocal images of immunohistochemistry for Iba1 (blue), C1q (green), CD47 (red) and VGluT1 (white), at P0, P5 and P10. Insert images shown at higher mag the area indicated by the dotted square. Yellow arrows indicate VGlut1 residues inside microglia tagged by C1q and/or CD47. Scale bar 5 μm.

Figure legends for supplementary figures

Supplementary figure 1. A) Confocal images of L4-L5 sections of P0 (top row) and P10 (bottom row) mice. Labeling ChAT (blue) and VGlut1 synapses (green) in WT, $C1q^{-/-}$, $C3^{-/-}$, $CD47^{-/-}$. Scale 50 μm. **B)** VGluT1 synapses number per MN soma at P1, P5 and P10 mice (N=3 mice per group). Number of somas, WT P1 n=18, P5 n=14 and P10 n=16; $C1q^{-/-}$ P1 n=12, P5 n=17 and P10 n=13. **C)** Analysis synaptic density in 0-50 μm proximal dendrites. mice (N=3 mice per group). Number of dendrites, WT P1 n=30, P5 n=24 and P10 n=30; $C1q^{-/-}$ P1 n=30, P5 n=24. **$p < 0.001$, ***$p < 0.001$; one-way ANOVA multiple comparisons with Bonferroni's test. **D) C**onfocal image of immuno for VGluT1 (white) and MN (blue) in P5 $C1q^{-/-}$ mouse. **E)** Electrical responses from ventral roots of WT and $C1q^{-/-}$ mice, with stimulations from dorsal roots in L4 or L5. Red trace despites mean of first 5 responses (grey). The arrowhead indicates stimulus artifact. The dotted lines indicate baseline. Blue arrows indicate peak amplitude mean. **F)** Amplitude of spinal reflexes at P5. WT, N=6; $C1q^{-/-}$, N=5. *$p < 0.05$, one-way ANOVA multiple comparisons with Bonferroni's test. **G)** Latency of responses for the same group as in (F) **H)** Double KO $C1q^{-/-}$::$CD47^{-/-}$ mice, P0 (left) and P10 (right). **I)** The total number of synapses on the entire soma comparing $C1q^{-/-}$, $CD47^{-/-}$, and $C1q^{-/-}$::$CD47^{-/-}$ double KO, at P0, P5 and P10. Number of somas, $C1q^{-/-}$ P1 n=12, P5 n=17 and P10 n=13; $CD47^{-/-}$ P1 n=15, P5 n=10 and P10 n=12; $C1q^{-/-}$::$CD47^{-/-}$ P1 n=4, P5 n=5 and P10 n=5. One-way ANOVA multiple comparisons with Bonferroni's test. **J)** Body weight from mice used to perform behavioral experiments **(r**ighting times Figure 1G). One-way ANOVA multiple comparisons with Bonferroni's test. **K)** Reproducibility of responses at 0.1 Hz (left) and 10 Hz (right), at P5. WT (blue line. 0.1 Hz N=4; 10 Hz N=3), $C3^{-/-}$ (green line. 0.1 Hz N=4; 10 Hz N=4), and $CD47^{-/-}$ (purple line. 0.1 Hz N=4; 10 Hz N=4). and **L)** P10. WT (blue line. 0.1 Hz N=8; 10 Hz N=8), $C3^{-/-}$ (green line. 0.1 Hz N=4; 10 Hz N=4), and $CD47^{-/-}$ (purple line. 0.1 Hz N=3; 10 Hz N=3). *$p < 0.05$, ***$p < 0.001$; two-way ANOVA multiple comparisons with Tukey's test.

Supplementary figure 2. A) Representative immuno of P5 PV::FlpO;Ai65, depicting TA MN innervating by homonymous proprioceptors. Single channels for DsRed (red), ChAT (blue), VGlut1 (grey), rAAV6/ds-CBH-GFP (green). Merged image (right), zoom-in correspond to dotted square area. Scale bars 50 μm. **B)** Identification of inappropriate synapses example. Image depicting an excluded synapse from analysis. DsRed (red), TA MN (green), and VGluT1 synapses (blue) from P5 PV::FlpO;Ai65 mouse. **C)** Confocal Zstack images of 3.5 μm from GA MN pool from PV::FlpO;Ai65 (left) and PV::FlpO;Ai65;$C3^{-/-}$ (right) injected with rAAV6/ds-CBH-GFP virus in GA and CAV2-CMV-Cre on TA. Representation of innapropiate synapses from gastro to tibialis anterior MN in PAC3 mouse. Scale 20 μm. **D)** Percentage of MN with innapropiate synapses from TA to gastro MNs. WT n= 2; $C3^{-/-}$ N=2. *$p < 0.05$; Unpaired t-test. **E)** Identification of innapropiate synapses in PV::FlpO;Ai65;$C1q^{-/-}$ (PAC) mice. Immuno for DsRed (red), VGluT1 (blue), and GFP (green). **F)** Percentage of total cells with inappropriate synapses on $C1q^{-/-}$ animals (left). WT (N=3) and $C1q^{-/-}$ (N=4). ***$p < 0.001$; Unpaired t-test.

Supplementary figure 3. A) Representative example of muscle activity traces in a $C1q^{-/-}$ mouse. Homonymous responses (top traces) and antagonistic muscle (bottom traces). Red traces despite of mean of first five responses (grey). Arrowhead identify electrical stimulation artifact, green arrow pointing homologues H reflex, and blue arrows point to inappropriate H reflexes. **B)** Latency of electrical recordings, M responses (empty circle), homonymous H reflex (empty square) and antagonistic H reflex (red circle). **C)** Amplitude analysis of homonymous H reflex (left) and antagonistic H reflex (right) from WT and $C1q^{-/-}$ mice. Each data point corresponds to a recording on GA or TA muscle, WT N=6, $C1q^{-/-}$ N=6. *$p < 0.05$; Unpaired t-test.

Supplementary figure 4. A) Schematic illustration for intracellular recordings in TA L4 MN incorporating him-limb preparations, using concentric needle electrodes for recording TA and GA muscles activity (grey), suction electrodes for ventral root L4-L5 (yellow), CP and tibial nerve electrodes for stimulation (green), and intracellular pipette filled with intracellular solution plus CTB594. **B)** Example of antidromic action potential recording in TA MN while stimulating in L4 ventral root, confirming MN from TA MN pool. Holding membrane potential -60 mV. Head arrow indicate the ventral root stimulation artifact. **C)** Passive electrical properties of TA MN using intracellular recordings. Membrane potential **D)** Input resistance **E)** Rheobase. From WT n=7 $C3^{-/-}$ n=5, and $CD47^{-/-}$ n=7. *$p < 0.05$, **$p < 0.001$, ***$p < 0.001$; one-way ANOVA multiple comparisons with Bonferroni's test. **F)** Rate of rise of currents from inappropriate synapses experiments. **G)** Single optical plane from confocal images of recorded cells, corresponding to Figure 4B. WT (top), $C3^{-/-}$ (middle), and $CD47^{-/-}$ (bottom). Cells labeled with neurobiotin (blue), and CTB488 (green). **H)** Frequency of firing from C3-/- and CD47-/- mice compare to WT. Stimuli correspond to 50 pA of increases after rheobase. **I)** CMAPs latency from experiments Figure 4A.

Supplementary figure 5. Representative recordings for the Jitter test in WT, $C3^{-/-}$, and $CD47^{-/-}$ mice. Experiments were performed at P5/7. Red arrow points the stimulus artifact. EPSPs from three different stimulation frequencies (0.1, 0.2 and 1Hz).

Supplementary figure 6. A) Single plane confocal images VgluT1 (red), CD47 (green) and ChAT positive cells, for a $C1q^{-/-}$ mouse. Scale bar 50 μm. **B)** Quantification of percentage of synapses tagging percentage by CD47 at P1, P5 and P10 in Soma. (N=3 mice per group). WT P1 n=18, P5 n=14 and P10 n=16; $C3^{-/-}$ P1 n=18, P5 n=17 and P10 n=16; $CD47^{-/-}$ P1 n=15, P5 n=10 and P10 n=12. **F)** Percentages of synaptic density on dendrites tagged by CD47. Number of dendrites, WT P1 n=30, P5 n=24 and P10 n=30; $C3^{-/-}$ P1 n=30, P5 n=30 and P10 n=30; $CD47^{-/-}$ P1 n=30, P5 n=20 and P10 n=30. *$p < 0.05$, **$p < 0.001$; one-way ANOVA multiple comparisons with Bonferroni's test.

Supplementary figure 7. A) Images from RNAscope plus immunohistochemistry experiments of $C1q^{-/-}$ P5 mice. Probe against CD47, merged image (left). Images corresponding to yellow doted squares and antibodies for Iba1 (green) (top), GFAP (bottom), MN identified with ChAT (blue) (middle images) and DAPI (grey). Scale bars 20 μm. **B)** Quantification of CD47 puncta per soma

in WT (P5, n=4; P10 n=5), C1q$^{-/-}$ (P5, n=5; P10 n=6), and control CD47$^{-/-}$ (P5, n=4; P10 n=3). ns = non-significant differences. ***p < 0.001; one-way ANOVA multiple comparisons with Bonferroni's test. **C)** Single plane of confocal images of RNAscope, identification of CD47 mRNA puncta expression in C3$^{-/-}$ mice at P5. on microglia but not in motor neurons of P10 mice. WT (top), CD47$^{-/-}$ (middle), and control C1q$^{-/-}$ mice (bottom). Iba1 (green) (top), GFAP (bottom). Scale bar 20 μm. **D)** Quantification of CD47 puncta per soma in WT (P5, n=4; P10 n=5), C1q$^{-/-}$ (P5, n=5; P10 n=6), and control CD47$^{-/-}$ (P5, n=4; P10 n=3). ns = non-significant differences. ***p < 0.001; one-way ANOVA multiple comparisons with Bonferroni's test.

Supplementary figure 8. A) Single plane confocal images of immunohistochemistry experiments performed from P5 WT mice showing the interaction of CD47 and Sirpα (CD47 receptor), on proprioceptive parvalbumin positive dendrites. Antibodies used were PV (green), CD47 (red), and Sirpα (blue). Merged image (bottom), while right image represents amplification of the dotted squares on the merge image. White arrows indicate examples of CD47 – Sirpα interaction on dendrites. **B)** Confocal image of SC LMC L4 level. Image despites interaction of CD47 and Sirpα (CD47 receptor), MN. Antibodies used were ChAT (green), CD47 (red), and Sirpα (blue). Merge image (bottom), while right images represent amplification of the dotted squares on the merge image. White arrows indicate examples of CD47 – Sirpα interaction on dendrites (top) and MN somas (bottom).

Figure 1.

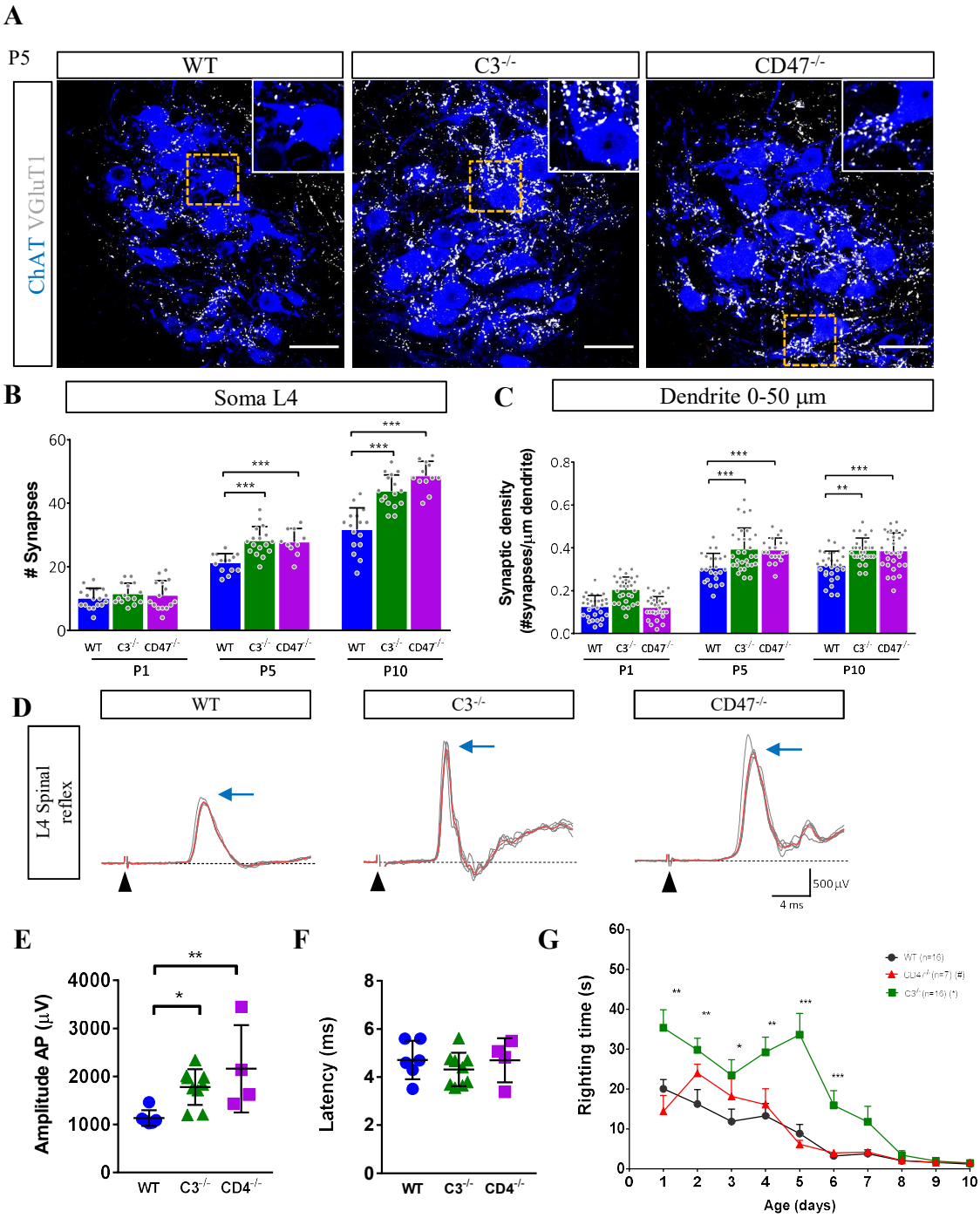
A
P5
WT
C3-/-
CD47-/-
ChAT VGluT1
B
Soma L4
Synapses
P1
P5
P10
C
Dendrite 0-50 µm
Synaptic density (#synapses/µm dendrite)
D
L4 Spinal reflex
500 µV
4 ms
E
Amplitude AP (µV)
F
Latency (ms)
G
Righting time (s)
Age (days)

Figure 2.

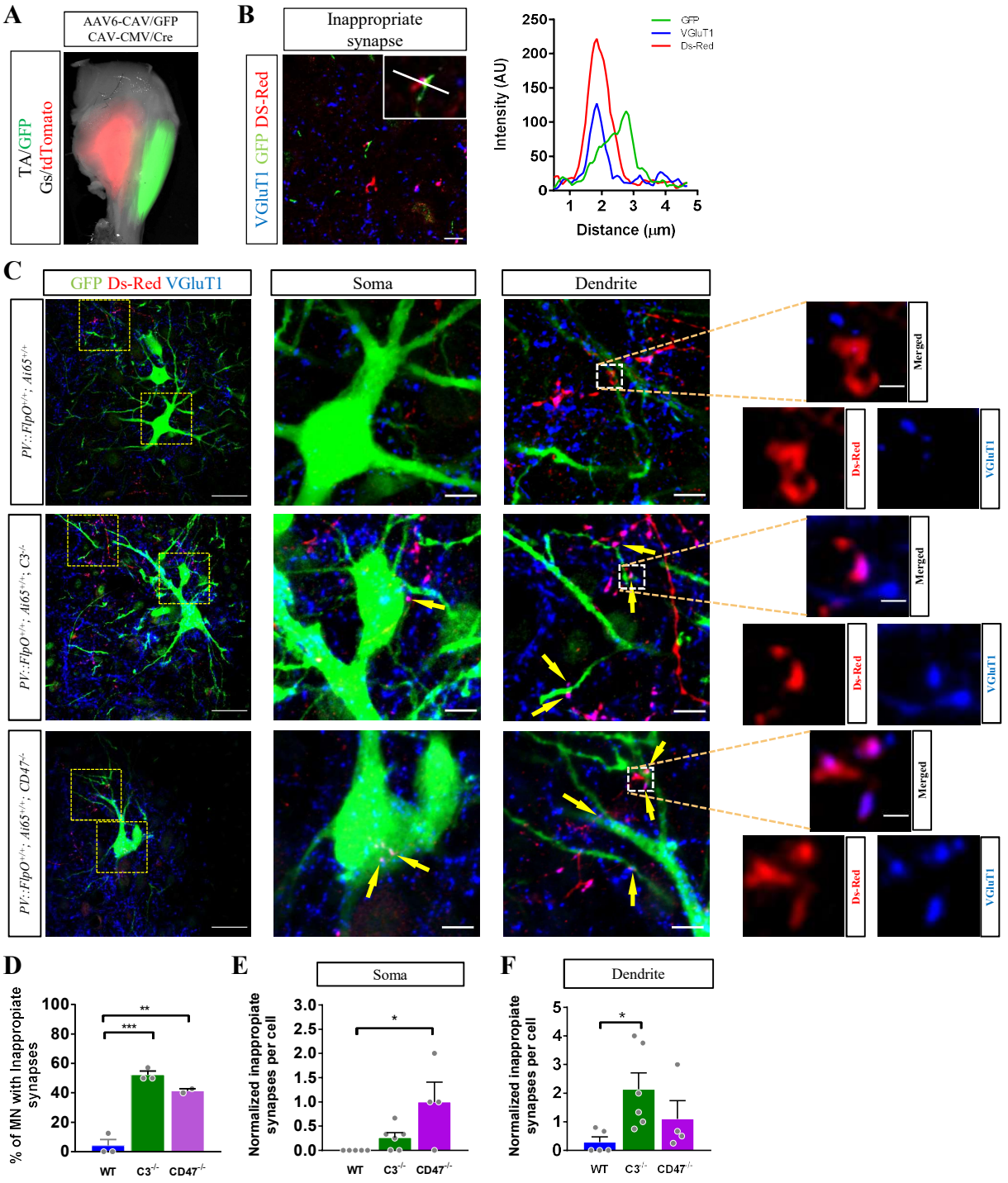
A
AAV6-CAV/GFP
CAV-CMV/Cre
TA/GFP
Gs/tdTomato
B
Inappropriate synapse
VGluT1 GFP DS-Red
GFP
VGluT1
Ds-Red
Intensity (AU)
Distance (μm)
C
GFP Ds-Red VGluT1
Soma
Dendrite
PV::FlpO+/+; Ai65+/+
PV::FlpO+/+; Ai65+/+; C3-/-
PV::FlpO+/+; Ai65+/+; CD47-/-
Merged
Ds-Red
VGluT1
D
% of MN with Inappropiate synapses
WT
C3-/-
CD47-/-
E
Soma
Normalized inappropiate synapses per cell
F
Dendrite

Figure 3.

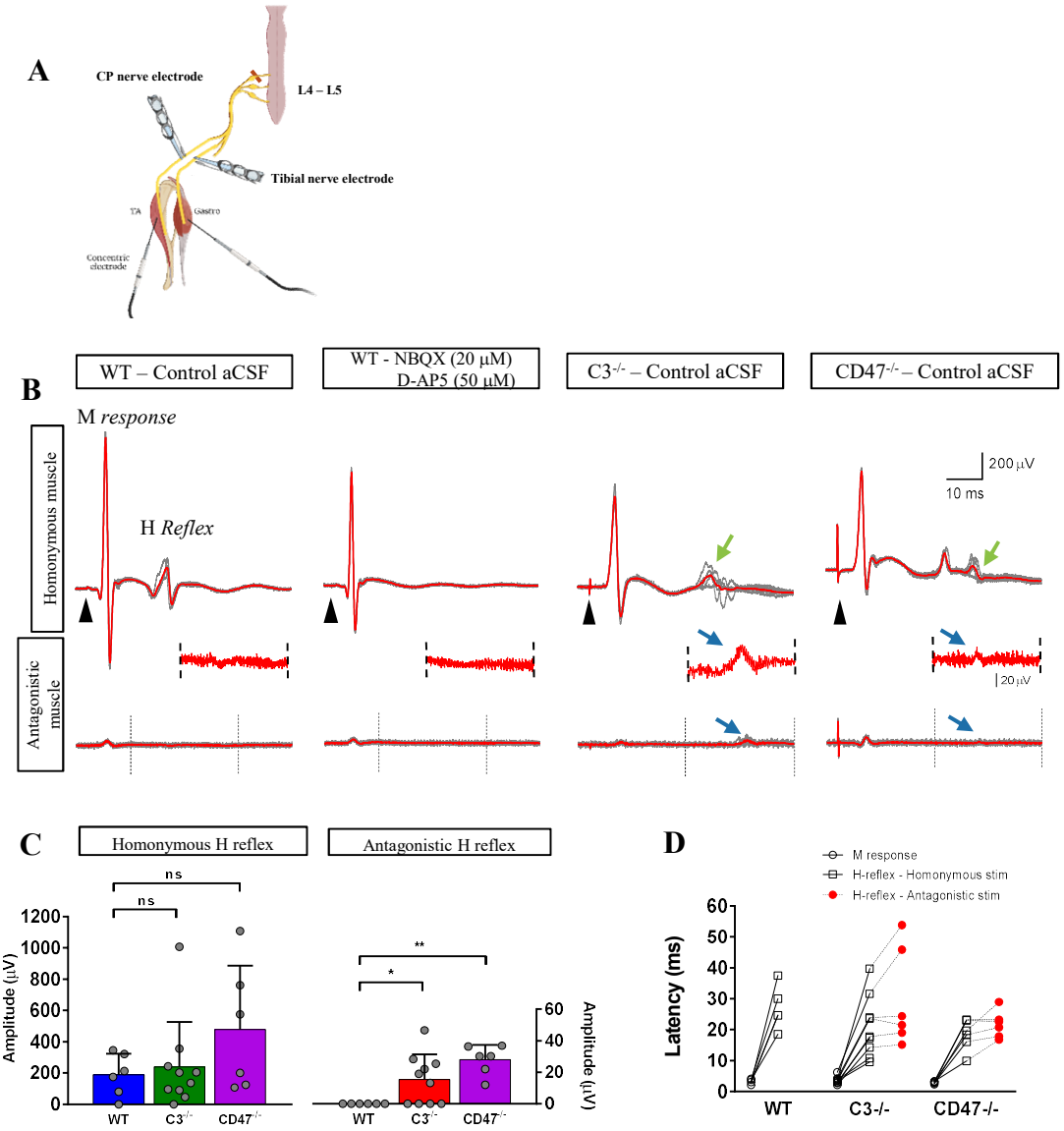
A
CP nerve electrode
L4 – L5
Tibial nerve electrode
TA
Gastro
Concentric electrode
B
WT – Control aCSF
WT - NBQX (20 µM) D-AP5 (50 µM)
C3-/- – Control aCSF
CD47-/- – Control aCSF
M response
H Reflex
Homonymous muscle
Antagonistic muscle
200 µV
10 ms
20 µV
C
Homonymous H reflex
Antagonistic H reflex
ns
ns
**
*
Amplitude (µV)
WT
C3-/-
CD47-/-
D
M response
H-reflex - Homonymous stim
H-reflex - Antagonistic stim
Latency (ms)
WT
C3-/-
CD47-/-

Figure 4.

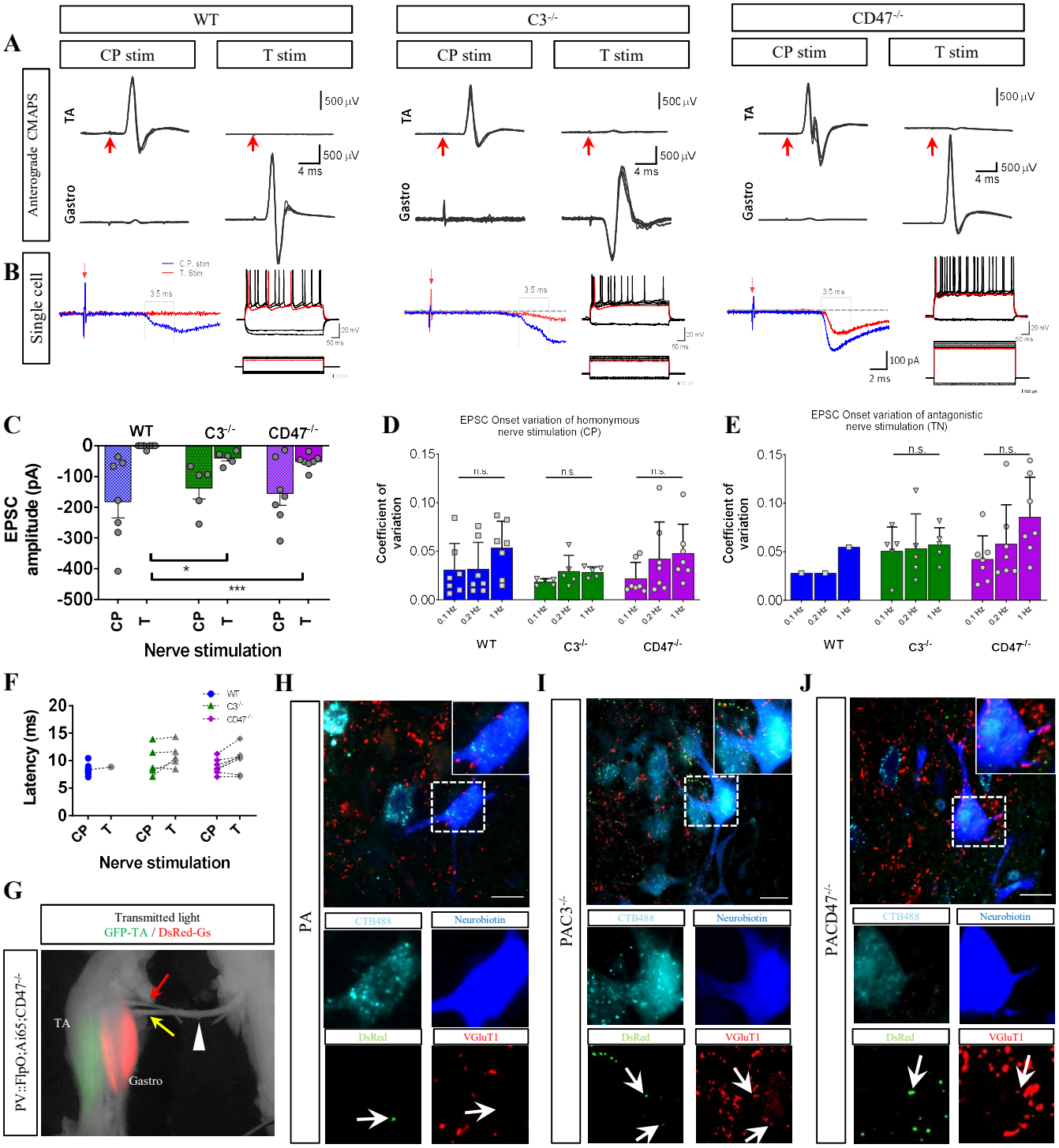
A
WT
C3-/-
CD47-/-
CP stim
T stim
Anterograde CMAPS
TA
Gastro
500 µV
4 ms
B
Single cell
C.P. stim
T. Stim
3.5 ms
20 mV
50 ms
100 pA
2 ms
C
EPSC amplitude (pA)
Nerve stimulation
D
EPSC Onset variation of homonymous nerve stimulation (CP)
Coefficient of variation
n.s.
0.1 Hz
0.2 Hz
1 Hz
E
EPSC Onset variation of antagonistic nerve stimulation (TN)
F
Latency (ms)
G
Transmitted light
GFP-TA / DsRed-Gs
PV::FlpO;Ai65;CD47-/-
H
PA
I
PAC3-/-
J
PACD47-/-
CTB488
Neurobiotin
DsRed
VGluT1

Figure 5.

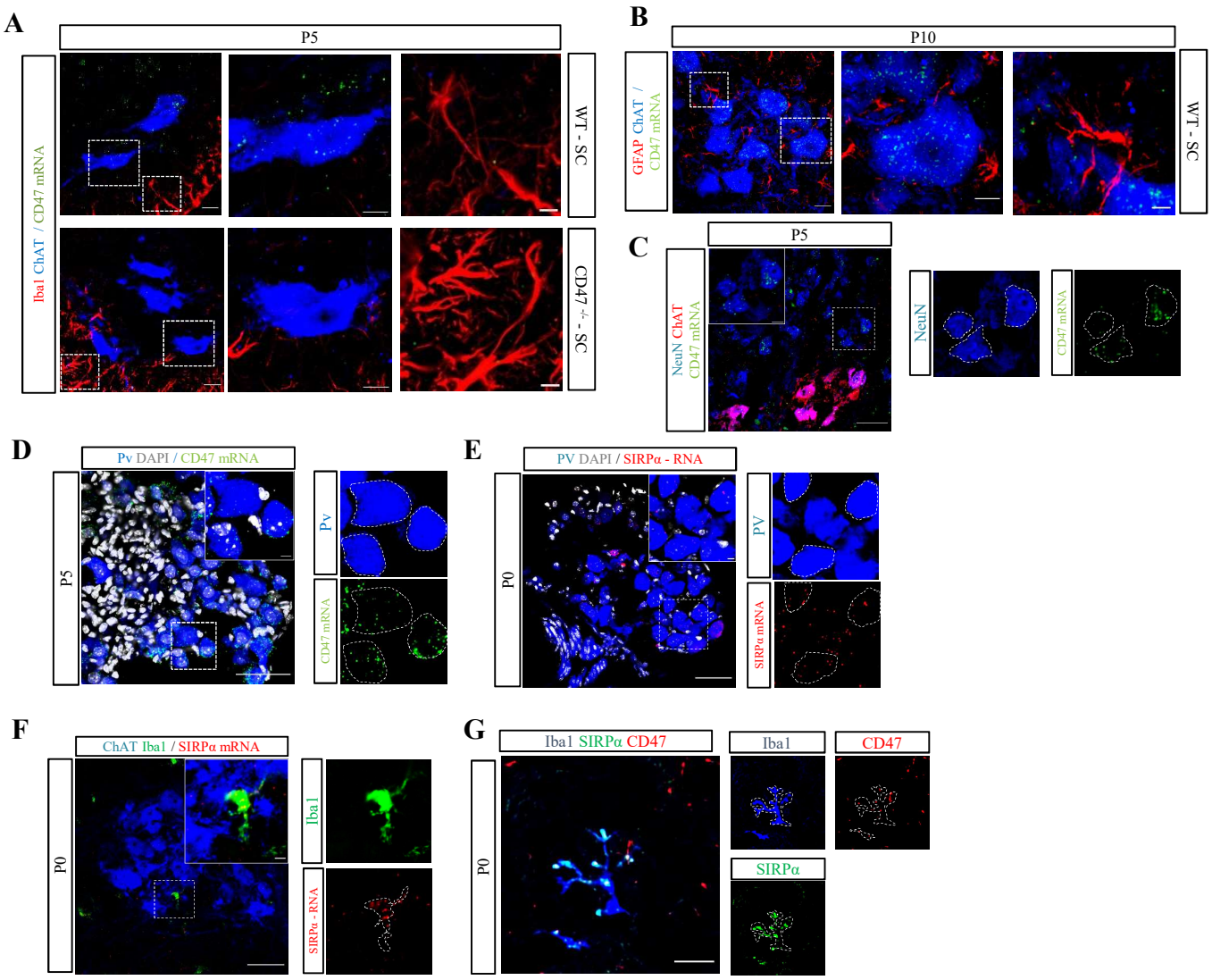
A
P5
Iba1 ChAT / CD47 mRNA
WT - SC
CD47 -/- - SC
B
P10
GFAP ChAT / CD47 mRNA
WT - SC
C
P5
NeuN ChAT CD47 mRNA
NeuN
CD47 mRNA
D
Pv DAPI / CD47 mRNA
P5
Pv
CD47 mRNA
E
PV DAPI / SIRPα - RNA
P0
PV
SIRPα mRNA
F
ChAT Iba1 / SIRPα mRNA
P0
Iba1
SIRPα - RNA
G
Iba1 SIRPα CD47
P0
Iba1
CD47
SIRPα

Figure 6.

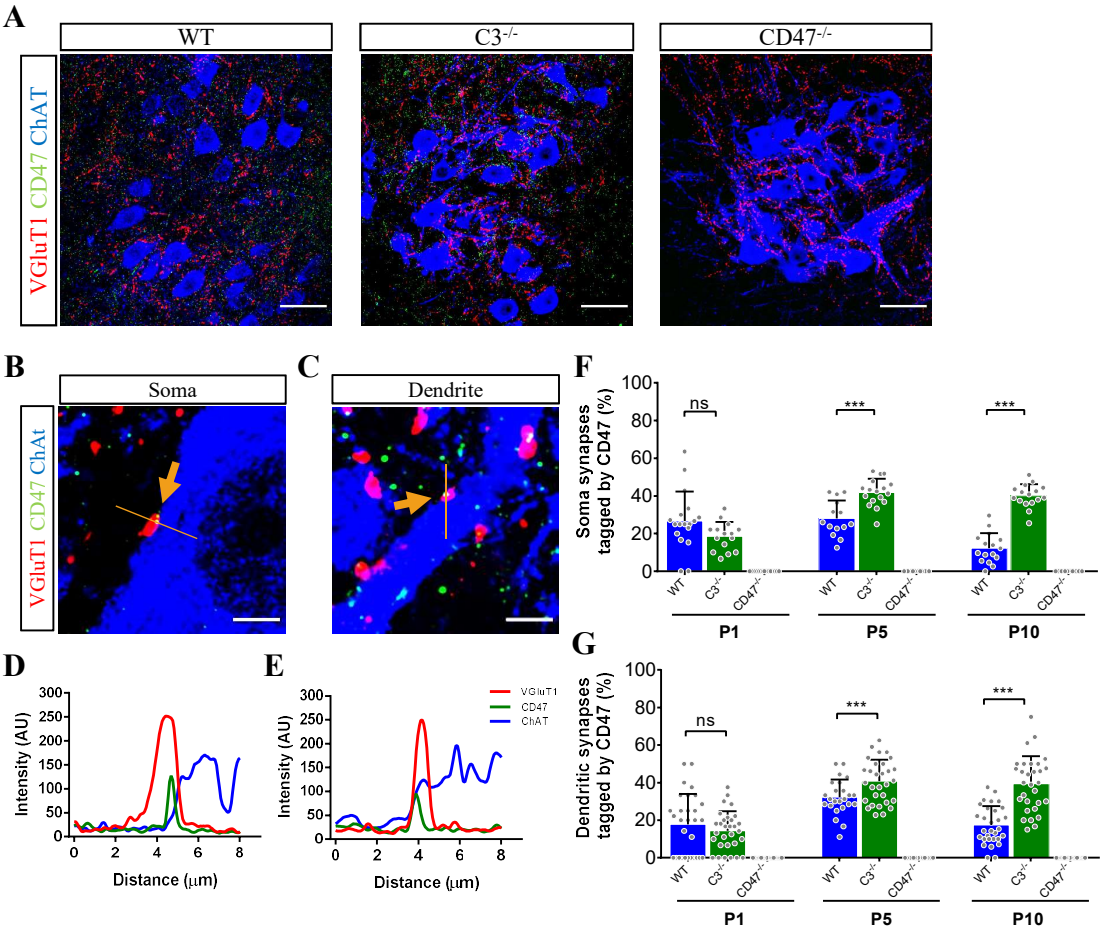
A
WT
C3-/-
CD47-/-
VGluT1 CD47 ChAT
B
Soma
C
Dendrite
VGluT1 CD47 ChAt
D
E
Intensity (AU)
Distance (μm)
VGluT1
CD47
ChAT
F
Soma synapses tagged by CD47 (%)
ns
***
P1
P5
P10
G
Dendritic synapses tagged by CD47 (%)

Figure 7.

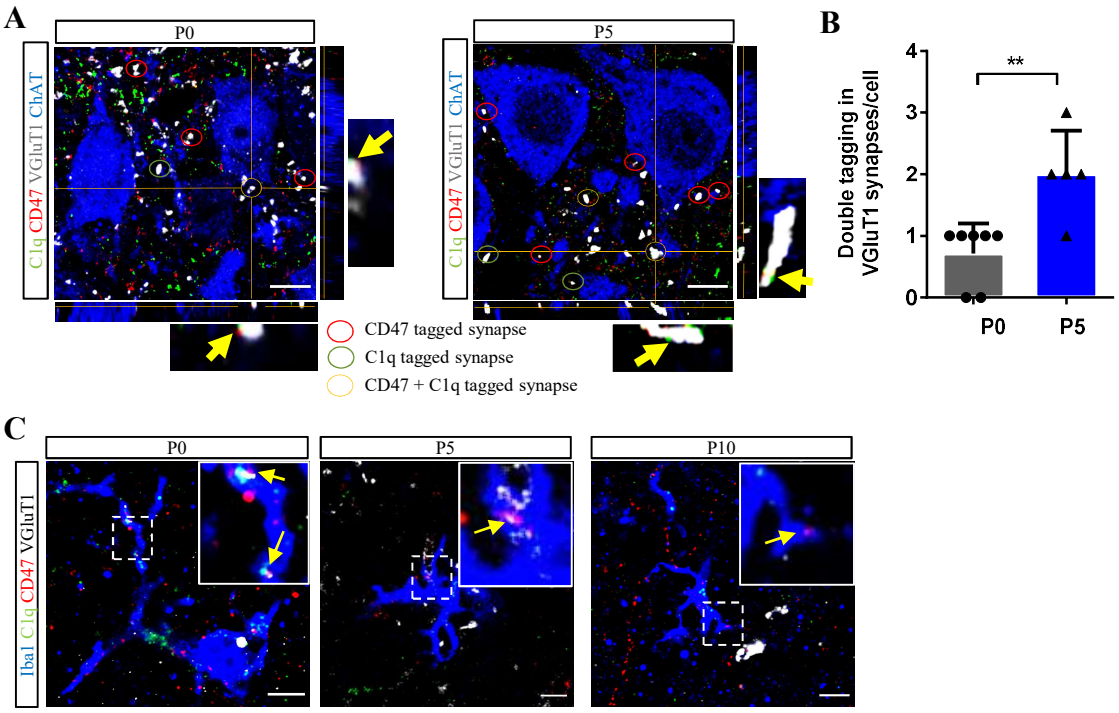
A
P0
P5
C1q CD47 VGluT1 ChAT
CD47 tagged synapse
C1q tagged synapse
CD47 + C1q tagged synapse
B
Double tagging in VGluT1 synapses/cell
**
P0
P5
C
P0
P5
P10
Iba1 C1q CD47 VGluT1

Supplementary

Supplementary Fig 1.

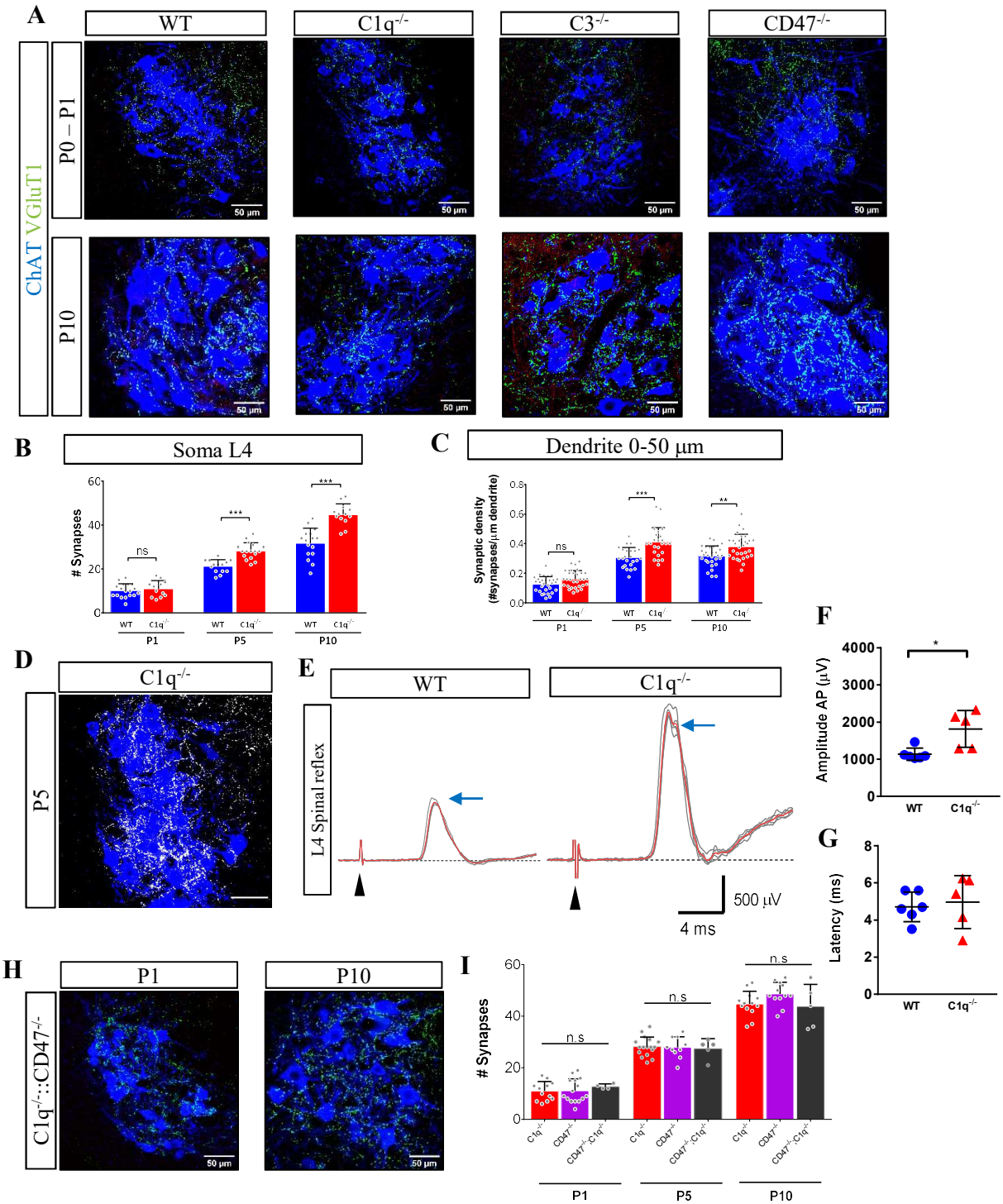

J

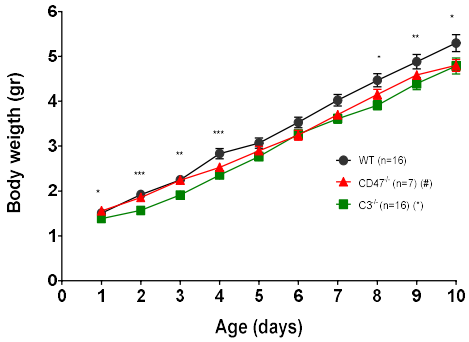
Body weigth (gr)
Age (days)
WT (n=16)
CD47-/- (n=7) (#)
C3-/- (n=16) (*)

K

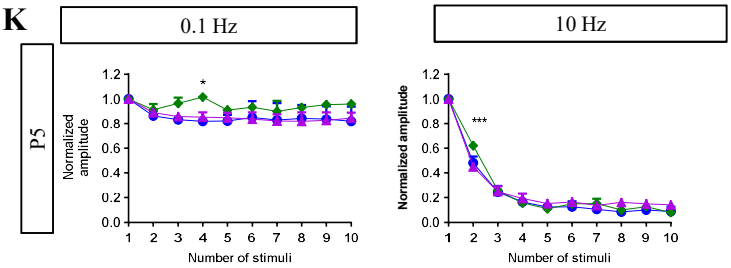
0.1 Hz
10 Hz
P5
Normalized amplitude
Number of stimuli

L

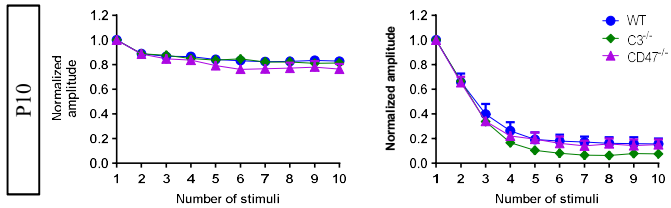
P10
Normalized amplitude
Number of stimuli
WT
C3-/-
CD47-/-

Supplementary Fig 2.

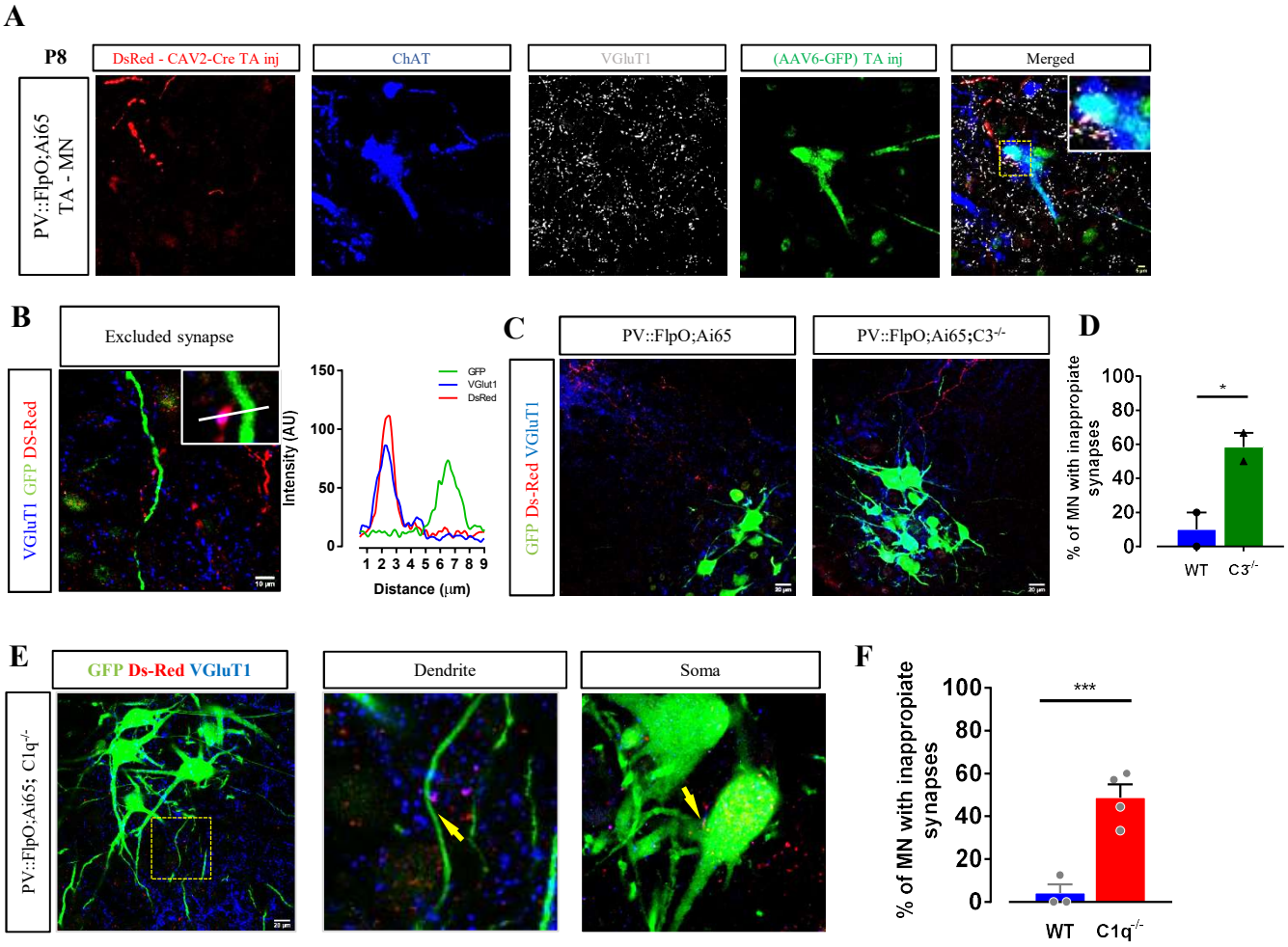

Supplementary Fig 3.

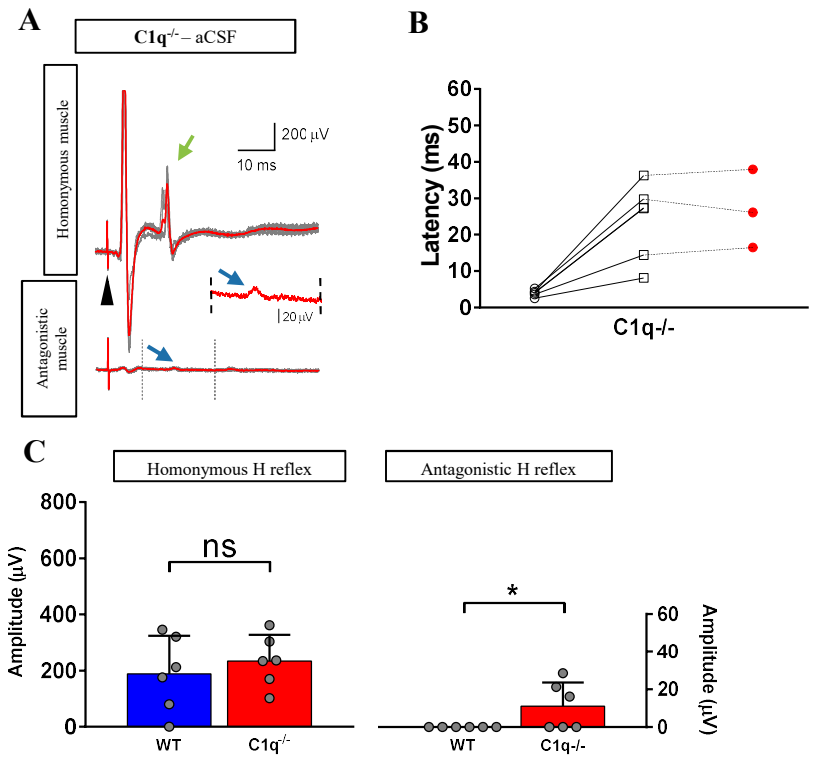

Supplementary Fig 4.

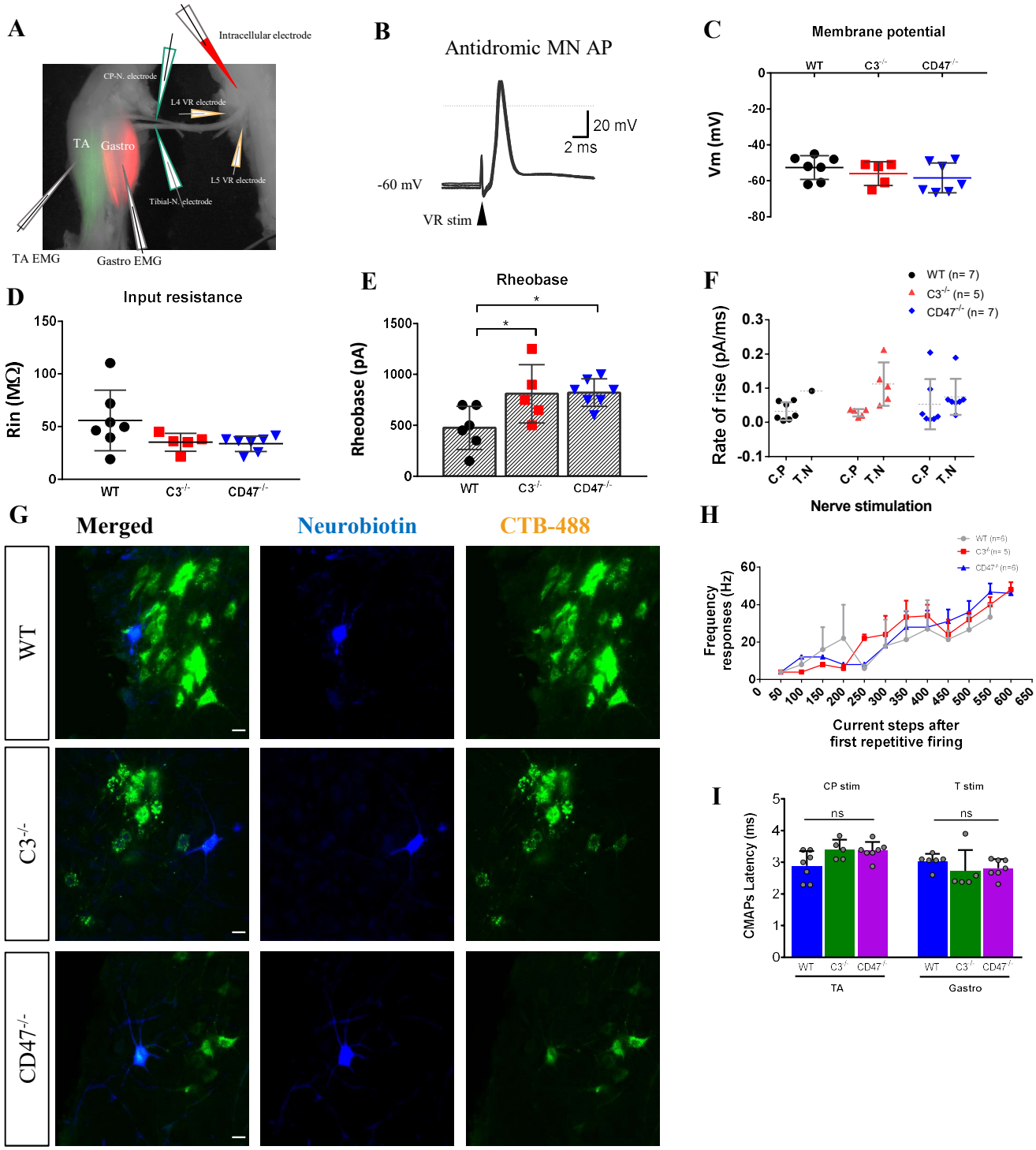

Supplementary Fig 5.

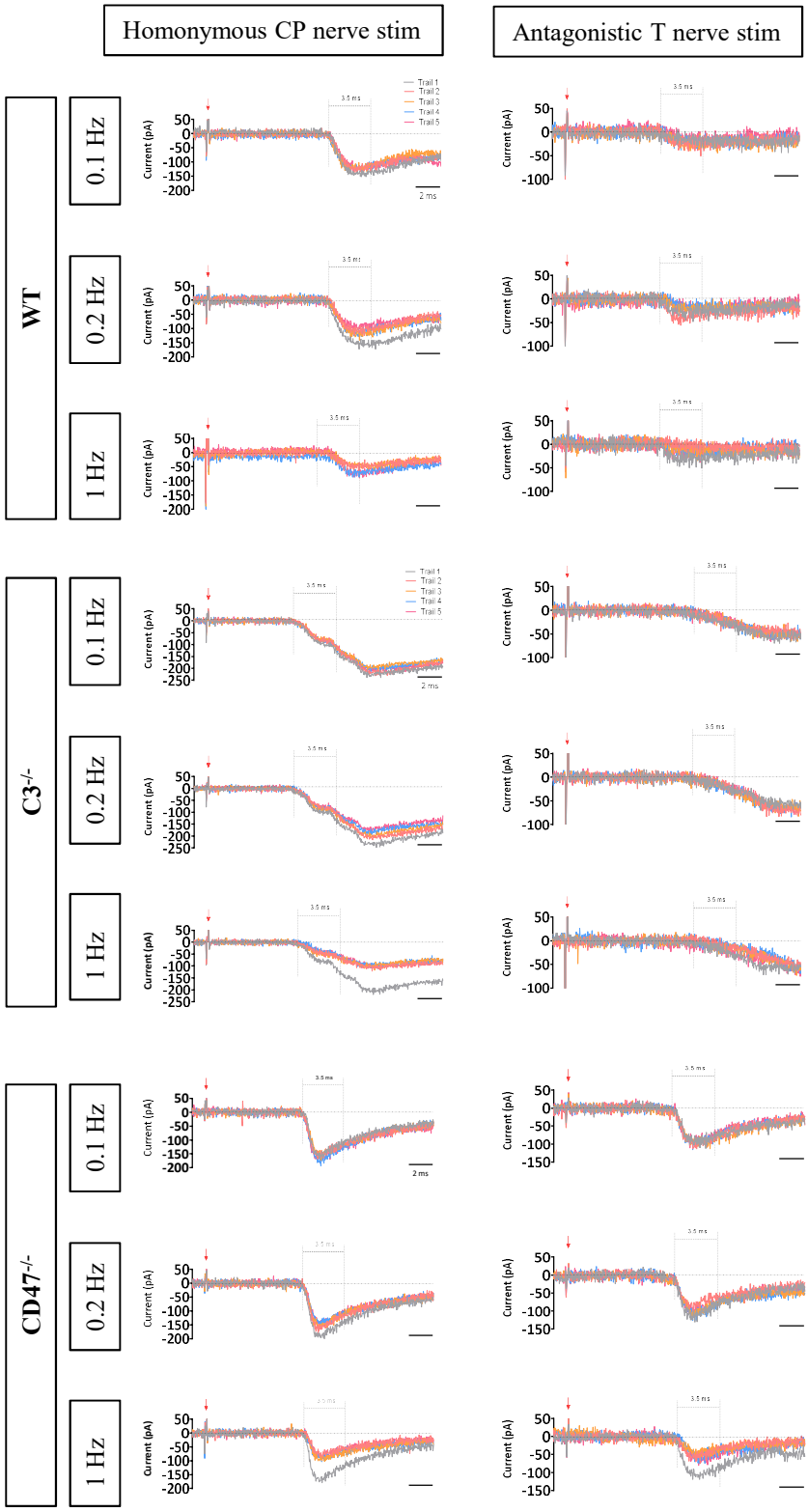

Supplementary Fig 6.

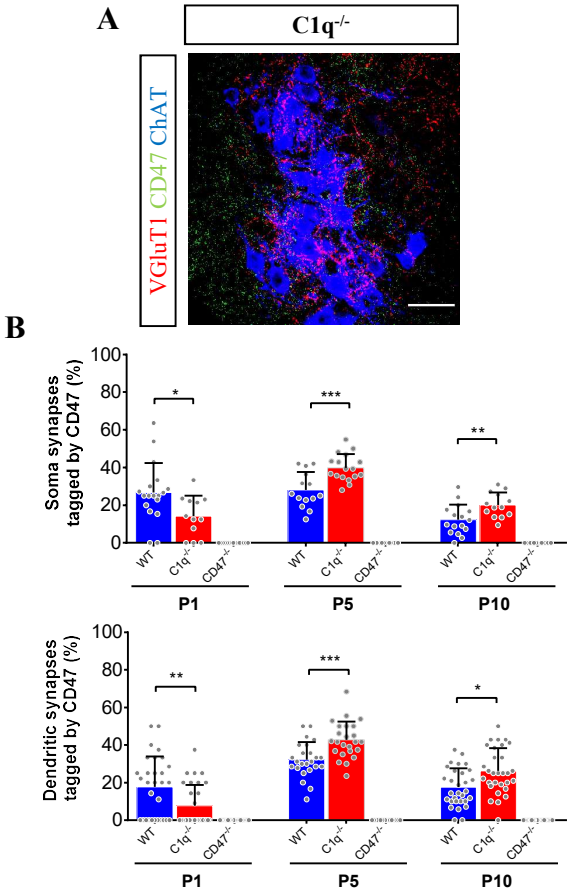

Supplementary Fig 7.

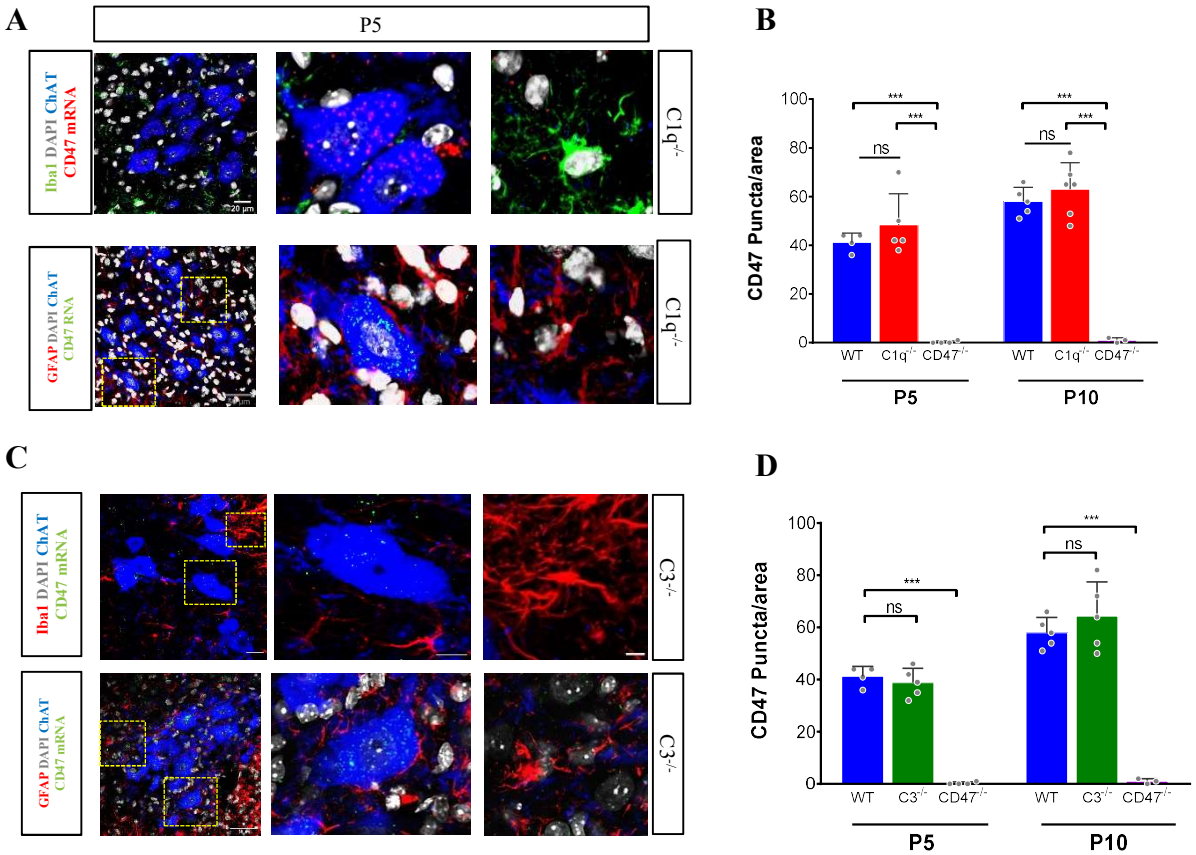
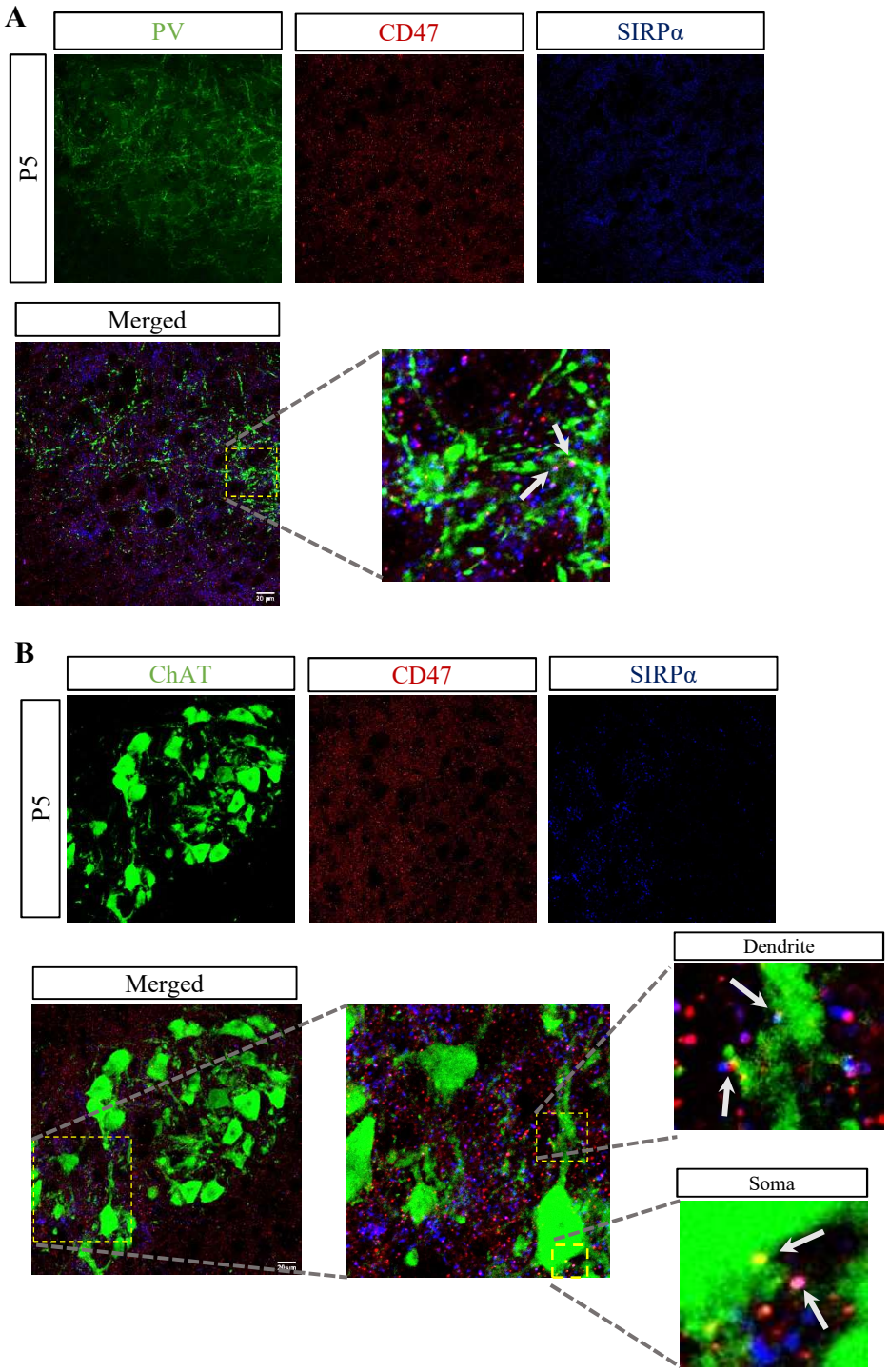
Supplementary Fig 8.